NASA Contractor Report 3482

Design for Active and Passive Flutter Suppression and Gust Alleviation

Mordechay Karpel

GRANT NGL-05-020-243
NOVEMBER 1981

NASA

NASA Contractor Report 3482

Design for Active and Passive Flutter Suppression and Gust Alleviation

Mordechay Karpel
Stanford University
Stanford, California

Prepared for
Langley Research Center
under Grant NGL-05-020-243

National Aeronautics
and Space Administration

Scientific and Technical Information Branch

1981

CONTENTS

TABLES

ILLUSTRATIONS

SUMMARY

Analytical design techniques for active and passive control of aeroelastic systems are presented. These techniques are based on a rational approximation of the unsteady aerodynamic loads in the entire Laplace domain, which yields matrix equations of motion with constant coefficients.

Some existing rational approximation schemes are reviewed, the matrix Padé approximant is modified, and a new technique which yields a minimal number of augmented states for a desired accuracy is presented.

The state-space aeroelastic model is used to design an active control system for simultaneous flutter suppression and gust alleviation. The design target is for a continuous controller which transfers some measurements taken on the vehicle to control command applied to a control surface. The control parameters are constant and they are optimized to minimize any desired combination of gust response parameters in a way that assures stability over the range of varying aerodynamic parameters in the entire flight envelope.

Structural modifications are formulated in a way which enables the treatment of passive flutter suppression system with the same procedures by which active control systems are designed.

INTRODUCTION

Background

In recent years, extensive research has been carried out to develop active control systems for controlling aeroelastic response. In these systems aerodynamic control surfaces are operated according to a control law which relates motion of the control surfaces to some measurements taken on the vehicle. The aerodynamic forces generated by the control surfaces modify the overall forces in some favorable way as defined by the performance requirements.

The increasing emphasis on fuel efficiency and the advances in aerodynamic and structural design techniques results in increasing payload to structural weight ratio. This increased structural efficiency results in lower elastic mode frequencies. Thus the elastic modes are more easily excited by atmospheric turbulence and pilot control inputs. Several development and flight test programs, such as the B-52 Load Alleviation and Mode Stabilization (LAMS) [1] and Drones for Aerodynamic and Structural Testing (DAST) [2], demonstrated aeroelastic control concepts for augmented rigid body stability, maneuver load control, ride control, fatigue reduction, gust alleviation and flutter suppression. The DAST program is still in progress and will continue for several years. The benefits of the aeroelastic control systems are increased aircraft maneuverablity, rider comfort, service life and flight envelope for a given structural layout.

Flutter suppression is fundamentally different from the other active control applications mentioned because the structural stability of the vehicle is involved. Loss of a flutter suppression control system may result in almost immediate major structural failure and the loss of the aircraft. Consequently, the active control system hardware must be of high reliability, and structural stability should be assured for all possible structural configurations in the entire flight envelope, extended to include safety margins. Some recent analytical developments, wind-tunnel tests and flight-test demonstrations [2-6] show the potential and feasibility of active flutter suppression control systems. However, to apply modern control techniques efficiently for optimized systems, more refined aeroelastic modeling has to be carried out.

The main difficulty in modeling an aeroelastic system for control analysis lies in the representation of the unsteady aerodynamic loads. The time lags in the development of these loads result in analytic expressions which contain non-rational terms. Rational approximations are needed to obtain finite-order models which can be solved by the methods of linear algebra.

Once a suitable approximation for the aerodynamic loads is chosen, a state-space matrix equation of motion can be constructed. Because aerodynamic loads are a function of flow conditions, each point in the flight envelope has a different equation of motion. A root-loci analysis yields the variation of the system frequencies of oscillation and damping ratios with the dynamic pressure for a given Mach number. After adding to the state-form equation, a control (input) term and a measurement (output) equation control, analysis is performed.

There is no all-purpose control technique. A suitable one is chosen in accordance with the performance requirements, available control means, precision of the mathematical model, measurement accuracy and on-board computer capacity. The control analysis given in this study is for a constant parameter, partial-feedback, continuous control system. A combination of modal and control surface response to atmospheric turbulence at various flight conditions is used as a cost function in such a way that stability is assured and a desired gust response parameter is minimized.

Structural modifications are more traditional aeroelastic control means. Passive compensators such as mass balance or stiffness tuning, with the associated weight penalty, can be more practical than active means in many instances and should not be overlooked in the design process. Passive means are formulated in this work as input and output terms such that they can be included in the active control design.

Survey of Literature

The scope of this work goes across several major topics such as aeroelasticity, structural dynamics, turbulence, control analysis and optimization. The literature survey given in this section is a selective review. Many other relevant books and papers appear in the literature.

The idea of using an active control system to move aerodynamic control surfaces for flutter suppression was pursued in the last decade by several aircraft manufacturers and research institutions. The B-52 CCV program was the first to demonstrate such a system in flight. This and

some other feasibility studies [7,8], wind tunnel tests [4,6] and flight tests [2,5,9] show the potential and feasibility of such systems.

The structural analysis methods needed for earoelastic analysis are reasonably well developed. For example, the infinite dimensional spaces required to describe exact motion of aeroelastic systems can be reduced to finite dimensional spaces by the technique of truncated normal modes [10]. Further, normal mode analysis of the structure can be done by the well-developed finite element method [11].

The unsteady aerodynamic loads due to an oscillaning wind section in incompressible, two-dimensional flow were first developed by Theodorsen [12]. Extensions of Theodorsen's derivation are given by Timman and Van der Vooren [13] for subsonic flow and by Garrick and Rubinow [14] for supersonic flow. A thorough review of these and other derivations, including Possio's integral equation for the pressure distribution on a two-dimensional typical section due to small oscillations of assumed modes and the corresponding integral equation for three-dimensional wings, is given by Bisplinghoff, Ashley and Halfman [10]. Among the numerical techniques for solving the integral equation for a three-dimensional wing in subsonic flow is the doublet-lattice method of Albano and Rodden [15].

The availability of analytical tools for calculating the aerodynamic influence coefficients for lifting surfaces in simple harmonic motion leads to the classical V-g method for predicting flutter boundaries [10,16,17]. The flight conditions at which the dumping g ceases to be negative defines the flutter condition.

Sears [18] developed convolution integrals for the unsteady aerodynamic loads due to arbitrary motion of a typical section in incompressible flow and generalized Theodorsen's function for arbitrary motion. Edwards [19,20] applied the Laplace transformation to Sears' expressions and generalized Possio's integral equation for arbitrary motion. He also presented the aeroelastic equations of motion in a way that manifests the benefits of rational approximations of the aerodynamic loads, especially when an active control system is used.

R. T. Jones [21] first introduced the use of rational Laplace transfer functions to approximate unsteady loads. The importance of such approximations increased with the progress in active control of aeroelastic systems. Roger et al. [3] used Padé approximants [22] separately for each term of the aerodynamic influence coefficient matrix. Roger [23] increased the approximation efficiency by using common denominator roots. Vepa [24] and Edwards [19,20] used matrix Padé approximants to deal with all the influence coefficients simultaneously.

The analytical tools for calculating the response of flexible airplanes to atmospheric turbulence are summarized by Pratt [25]. The mechanism and theory of turbulence are given by Hinze [26]. Dryden [27] and von Karman [28] gave practical formulas for the statistical description of atmospheric gust velocity.

Like any other component of a flight vehicle, an active control system must comply with the Federal Aviation Regulations [29]. An example of regulation considerations for an active flutter margin augmentation system is given by O'Connell and Messina [9].

Aeroelastic active control design concepts are functions of the available aeroelastic modeling techniques. Nissim [30] developed the aerodynamic energy concept, which is based on the classical assumption of simple harmonic motion. This concept was applied by Nissim and Abel [4] and Abel et al. [31].

Rational approximations of the unsteady loads have been used to construct finite state-space mathematical models. Classical control techniques [31,32] and optimal control techniques [19,32] have been used to design flutter-suppression systems. The concepts and methodology of optimal control theory are given by Bryson and Ho [34]. Ashkenazi [35] applied some of these concepts to the constant parameter insensitive control of a system with variable dynamics.

When control parameters are optimized with respect to a given cost function, and there is no direct algebraic optimal solution, a minimization procedure can be used. Fletcher and Reeves [36] introduce the conjugate gradients technique. Davidon [37] introduced a rapidly convergent descent method which has been modified by Fletcher and Powell [38] and by Steward [39] to include finite difference approximation of the gradient vector.

The costs and benefits in using active control system to suppress flutter and alleviate gust response must demonstrate superiority over the more traditional passive flutter-suppression means. Structural optimization procedures for satisfying flutter requirements are given by Markowitz [40] and Haftka and Starnes [41]. The decoupler pylon concept, which avoids violating the flutter requirements when an external store is added to the wing, was developed by Reed et al. [42].

Report Outline

In the Aeroelastic Equations of Motion Section the typical section in incompressible and subsonic flow is introduced first. Unsteady aerodynamic loads in three-dimensional flow are discussed, and the use of truncated normal modes is presented.

In the Flutter and Gust Response Section the V-g method and the root-loci approach for calculating flutter boundaries are presented. The continuous gust loads and the associated structural dynamic response are defined in statistical terms, and the basic relations are given.

In the Finite State-Space Modeling Section the initial theoretical developments original to this work are presented. Some existing techniques for rational approximation of the aerodynamic loads are reviewed, the matrix Padé approximant is modified, and a new minimum-state technique is developed. Numerical examples for approximating two-dimensional aerodynamics in incompressible and subsonic flow and three-dimensional aerodynamics in subsonic flow are given.

In the Active Flutter Suppression and Gust Alleviation Section active control of aeroelastic systems is treated. Design targets are defined, some existing techniques are reviewed, and a new approach for simultaneous flutter suppression and gust alleviation is developed and illustrated.

In the Passive Flutter Suppression Section a new approach to passive means for flutter suppression is presented. The passive means are formulated as input and output terms of the active control equations. Numerical examples of stabilizing the typical section using a concentrated mass and a dynamic vibration absorber are given.

In the final two sections, Concluding Remarks and Recommendations, the material presented in this paper is summarized and recommendations for

future research presented.

Summary of Contributions

1. Rational approximations of the unsteady aerodynamic influence coefficients are investigated, the matrix Padé technique is modified and a new "minimum-state" technique is developed. Numerical examples are used to demonstrate significant advantages of the minimum-state technique over other techniques.

2. The minimum-state approximation is used to construct state-space aeroelastic control equations with flight-condition dependent coefficients. Statistical turbulence parameters are formulated as process noise.

3. A control cost function is defined such that a desired gust response parameter is minimized and stability over the entire flight envelope is achieved, if at all possible with the available control means.

4. A pole-assignment technique for a partial-feedback, zero-order compensator is modified to accommodate simultaneous pole assignments at different flight conditions.

5. Higher than zero-order compensators are augmented to the aeroelastic control equations, and the output equation includes an input term to accommodate acceleration measurements.

6. Passive control means are formulated as input and output terms such that they can be treated as a special case of active control means.

SYMBOLS

a	dimensionless elastic axis location (Fig. 1)
a_0	speed of sound
$a_{g,i}$	cost function weights, Eq. (5.16)
a_u	control command participation in z_d, Eq. (5.14)
b	reference semichord
b_p	viscous damping
c	dimensionless control surface hinge location (Fig. 1)
C_{ℓ_α}	lift coefficient derivative with respect to angle of attack, $L_\alpha/2bq$
$C(s')$	generalized Theodorsen function (Eq. (2.12))
$D_o(s)$	open-loop characteristic polynomial
$f(x_1),g(x_1)$	coefficients of spacial longitudinal and vertical velocity correlation, Eq. (3.11)
g	structural damping
h	plunge displacement (Fig. 1), altitude in Fig. 2
$H_n^{(2)}(z)$	Hankel function of order n
$Im(\bullet)$	imaginary part of $\bullet$
J_e	least-squares cost function, Eq. (4.2)
J_o	global control cost function, Eq.(5.16)
$J_n(z)$	Bessel function of order n
k	reduced frequency, $\omega b/V$
k_c	integer defined in Eq. (5.5)
k_p	spring stiffness

$K_n(s')$	modified Bessel function of order n
l_c	compensator order
L	lift per unit span
L_α	lift per unit span due to unit pitch angle
L_g	scale of turbulence, length units
m	order of the denominator polynomial in a rational approximation
m_c	number of output measurements
m_p	concentrated mass
m_s	wing mass per unit span
M	Mach number
M_α, M_β	pitching and hinge moments (Fig. 1)
n	number of degrees of freedom
n_c	order of control equation (5.1)
N	order of Roger's approximation, Eq. (4.5)
p	pressure difference across the wing
p''	amplitude of p
q	dynamic pressure, $\frac{1}{2}\rho V^2$
Q_i	polynomial coefficients of $D_0(s)$, Eq. (5.21)
r	magnitude of $s' = r \exp(i\theta)$
r_α^2, r_β^2	radius of gyration of the typical section and the control surface, divided by b
Re(•)	real part of •
s	Laplace transform variable
s'	nondimensionalized Laplace variable, sb/V
t	time
T_i	constants defined in Eq. (A.2)

$u, U(s)$	control command variable and its Laplace transform
u', v', w'	disturbance velocity components in x_1, y_1 and z_1 directions, respectively
u_g, w_g	vertical and longitudinal gust velocity
V	airspeed
w''	amplitude of w'
x_1, x_1, z_1	streamwise, spanwise and upwards spacial coordinates
x_{te}	x_1 coordinate of the trailing edge
x_α, x_β	dimensionless center of mass offsets (Fig. 1)
$Y_n(z)$	Bessel function of order n
z	defined in Eq. (A.4)
z_s	z_1 coordinate on the wing surface
$z_d, Z_d(s)$	gust response design variable and its Laplace transform
α	angle of attack
β, β_c	control surface actual and command rotations
γ_j	aerodynamic roots (Eq. (4.5))
$\Gamma(n)$	gamma function
ε	error of least-squares approximation
δ	concentrated mass location, Fig. 18
$\Phi_{wg}(\omega)$	power spectral density of w_g
Φ'	disturbance velocity potential
Ψ	modal deflection
λ	wave length of sinusoidal gust
μ	mass ratio, $m_s/\pi\rho b^2$
ρ	air density
σ_{wg}^2	mean-square value of w_g

$\sigma_{zd,i}^2$	mean-square value of z_d at point i of the flight envelope
θ	argument of s'
ω	vibration frequency, rad/sec
$\omega_h, \omega_\alpha, \omega_\beta$	plunge, pitch and flap uncoupled natural frequencies
ω_n	natural frequency
Ω	aeroelastic eigenvalues defined in Eq. (3.2)
ζ	modal damping

Matrices

adj[•]	adjoint matrix of [•]
$[a_d], [a_o], [a_v]$	frequency response coefficients in Eq. (3.10)
[A(s')]	aerodynamic influence coefficients
$[A_{ap}]$	approximated value of [A(s')]
$[A_c], [B_c]$	compensator parameter matrices, Eq. (5.5)
$\{A_g\}$	gust loads influence coefficients
$[A_{j,1}], [B_{j,1}]$	as defined in Eq. (4.12)
$[A_1], [B_1]$	known data matrices in Eq. (4.1)
[B]	damping matrix
$[B_1]$	defined in Eq. (4.15)
$[C], [C_c]$	control gains, Eq. (5.7)
$[C'], [c_c']$	defined in Eq. (5.8)
$[C(R', k_1)]$	as defined in Eq. (4.27)
$[C_z]$	defined in Eq. (5.12)
$[D], [D']$	defined in Eqs. (4.23) and (4.25)
$[D_1], [D_2]$	defined in Eqs. (4.15) and (4.18)
$[E], [E']$	defined in Eqs. (4.22) and (4.25)
$[E_i]$	defined in Eqs. (4.15) and (4.18)
[F(k)], [G(k)]	real and imaginary parts of [A(ik)]

$[F_1]$	dynamic matrix of aeroelastic control system, Eq. (5.1)
$\{g(s)\}$	as defined in Eq. (5.19)
$\{G_1\},\{G_2\}$	control input distribution vectors, Eq. (5.1)
$[H],\{J\}$	output matrices of Eq.(5.2)
$[H_a],[H_d],[H_v]$	partitions of [H], Eq. (5.2)
$[H_0]$	acceleration output matrix, Eq. (5.3)
$[I]$	unit matrix
$[K],[M]$	stiffness and mass matrices
$[K_1],[K_2]$	defined in Eq. (4.15) and (4.22)
$\{L_a(t)\},\{L_a(s)\}$	aerodynamic load vector and its Laplace transform
$[N_i]$	matrix polynomial coefficients in Eq. (5.20)
$[P_i]$	coefficients of matrix polynomial approximation
$[Q_{pt}]$	piston theory limit, page 110 of Ref. [16]
$[R]$	approximation root matrix, Eqs. (4.9) and (4.25)
$[R']$	defined in Eq. (4.24)
$\{R_1\},[S_1],[S_2]$	defined in Eq. (A.2)
$[T]$	similarity transformation matrix, Eq. (4.16)
$\{x\},\{X(s)\}$	deflections in generalized coordinates and their Laplace transform
$\{x_a\},\{x_{a1}\},\{x_{a2}\}$	aerodynamic augmented state vectors
$\{y\},\{Y(s)\}$	measurement vector and its Laplace transform
$\{z\},\{Z(s)\}$	state vector and its Laplace transform
$\{z_c\}$	compensator state vector
$\{\Psi_p\}$	modal deflection vector
$\{\Gamma\}$	noise distribution vector, Eq. (5.10)

Subscripts

a	aerodynamic

d	design
e	related to least-squares problem, Eq. (4.1)
eq	equivalent
f,f1,f2	l values at which approximated and tabulated terms match
i,j	of i-th and j-th mode, respectively
$[\bullet_{,i,}]$	row i of [•]
$\{\bullet_{,j}\}$	column j of [•]
$\bullet_{,ij}$	ij-th element of [•]
l	index of tabulated data
mo	maximum operation
nc	noncirculatory aerodynamic
p	passive
r1,r2	reference values of l in the least-squares equations
s	structural
sl	sea level

Superscripts

t	matrix transpose
-	average value

Abbreviations

C.G.	center of gravity
DOF	degrees of freedom
CCV	control configured vehicle
E.A.	elastic axis
FAA	Federal Aviation Administration
kPa	kilo-Pascal, 10^3 Newton/m^3

AEROELASTIC EQUATIONS OF MOTION

Unsteady Aerodynamics

The development of the partial differential equation for unsteady potential flow is presented in numerous textbooks and papers. An overall, thorough presentation is given by Bisplinghoff *et al*. [10]. The linearized partial differential equation for unsteady, compressible flow reads

$$\nabla^2\Phi' - \frac{1}{a_0^2}\left[\frac{\partial^2\Phi'}{\partial t^2} + 2V\frac{\partial^2\Phi'}{\partial x_1 \partial t} + V^2\frac{\partial^2\Phi'}{\partial x_1^2}\right] = 0 \qquad (2.1)$$

where Φ' is the disturbance velocity potential. The disturbance velocity components are

$$u' = \frac{\partial\Phi'}{\partial x_1} \quad , \quad v' = \frac{\partial\Phi'}{\partial y_1} \quad , \quad w' = \frac{\partial\Phi'}{\partial z_1} \qquad (2.2)$$

where x_1, y_1 and z_1 are the streamwise, spanwise and vertical coordinates, respectively, when flow over a wing is studied. The associated disturbance velocities u', v' and w' are assumed to be small compared to V.

For the unsteady lifting part of the solution of (2.1), a thin wing is replaced by its "flat plate" projection on the x_1-y_1 plane. The linearized condition of no flow across the wing provides the primary boundary condition of (2.1),

$$w'(x_1,y_1,0,t) = \frac{\partial z_a}{\partial t} + V\frac{\partial z_a}{\partial x_1} \tag{2.3}$$

where z_a is the local z_1 coordinate of the wing.

The unsteady flow is antisymmetric with respect to the x_1-y_1 plane. The pressure difference across the wing is

$$p(x_1,y_1,t) = -2\rho\left[V\frac{\partial}{\partial x_1} + \frac{\partial}{\partial t}\right]\Phi'(x_1,y_1,0^+,t) \tag{2.4}$$

Kutta's hypothesis of smooth flow off a sharp subsonic trailing edge requires that $p(x_{te},y_1,t) = 0$. Substituting $x_1 = x_{te}$ in Eq. (2.4) gives another boundary condition for Eq. (2.1),

$$\left[V\frac{\partial}{\partial x_1} + \frac{\partial}{\partial t}\right]\Phi'(x_{te},y_1,0,t) = 0 \tag{2.5}$$

In incompressible flow, Eq. (2.1) reduces to Laplace's equation,

$$\nabla^2\Phi' = 0 \tag{2.6}$$

The solution of Eq. (2.1) or (2.6) has traditionally been simplified by assuming that the wing is undergoing simple harmonic motion, thus removing the independent variable t. Further simplification can be made if two-dimensional flow is assumed, thus removing the independent variable y_1.

For oscillatory motion, $w'(x_1,y_1,0,t) = w''(x_1,y_1)\exp(i\omega t)$ and $p(x_1,y_1,t) = p''(x_1,y_1)\exp(i\omega t)$. For three-dimensional flow, Eqs. (2.1), (2.3) and (2.4) combine to the integral equation,

$$\frac{w''(x_1,y_1;k)}{V} = \frac{1}{8\pi}\iint_S \frac{p''(\xi,\eta;k,M)}{q} K(x_1-\xi,y_1-\eta;k,M)\,d\eta\,d\xi \qquad (2.7)$$

where ξ and η are dummy variables corresponding to x_1 and y_1, respectively, and $k = \omega b/V$ is the reduced frequency.

Landahl [43] gives an expression for the kernel function for nonplanar surfaces in subsonic flow. To simplify the formulation, the discussion here is limited to planar surfaces, for which the expression for the kernel function is

$$K = \frac{\exp[-ik(x_1-\xi)/b]}{(y_1-\eta)^2}\left[\frac{M|y_1-\eta|}{\sqrt{(x_1-\xi)^2+(1-M^2)(y_1-\eta)^2}}\,\frac{\exp[-ik|y_1-\eta|/b]}{\sqrt{1+u_1^2}} + \int_{u_1}^{\infty}\frac{\exp[-iku|y_1-\eta|/b]}{(1+u^2)^{3/2}}\,du\right] \qquad (2.8)$$

where $$u_1 = \frac{M\sqrt{(x_1-\xi)^2+(1-M^2)(y_1-\eta)^2}-(x_1-\xi)}{(1-M^2)|y_1-\eta|}$$

Knowing $w''(x_1,y_1;k)$, Eq. (2.7) is solved for $p''(x_1,y_1;k,M)/q$. Although this equation contains singularities, a solution can be obtained by numerical methods such as the doublet-lattice method [15].

The Typical Section

The typical section is a simplified aeroelastic system consisting of a rigid plate of unit span connected to the ground by springs. It has a

trailing-edge flap and is exposed to two-dimensional flow as shown in Fig. 1. Assuming no structural damping, the system equation of motion is

$$[M_s]\{\ddot{x}\} + [K_s]\{x\} = \{L_a(t)\} \tag{2.9}$$

where the displacement vector $\{x\}^t = [h/b, \alpha, \beta]$, the aerodynamic load vector $\{L_a\}^t = [-Lb, M_\alpha, M_\beta]$ and $[M_s]$ and $[K_s]$ are the structural mass and stiffness matrices

$$[M_s] = m_s b^2 \begin{bmatrix} 1 & x_\alpha & x_\beta \\ x_\alpha & r_\alpha^2 & r_\beta^2 + x_\beta(c-a) \\ x_\beta & r_\beta^2 + x_\beta(c-a) & r_\beta^2 \end{bmatrix}$$

$$[K_s] = m_s b^2 \begin{bmatrix} \omega_h^2 & 0 & 0 \\ 0 & r_\alpha^2 \omega_\alpha^2 & 0 \\ 0 & 0 & r_\beta^2 \omega_\beta^2 \end{bmatrix}$$

The unsteady aerodynamic loads for incompressible, two-dimensional flow were formulated by Theodorsen [12]. The solution of Eq. (2.6) yields the pressure distribution due to oscillatory motion in plunge h pitching and control surface rotation β. Integration over the chord gives down-load -L, pitching moment, M_α and hinge moment M_β per unit span.

Following Sears [18], Edwards [19] showed that these results may be generalized for arbitrary motion. The Laplace transform of $\{L_a(t)\}$ is

$$\{L_a(s)\} = q[A(s')]\{X(s)\} \tag{2.10}$$

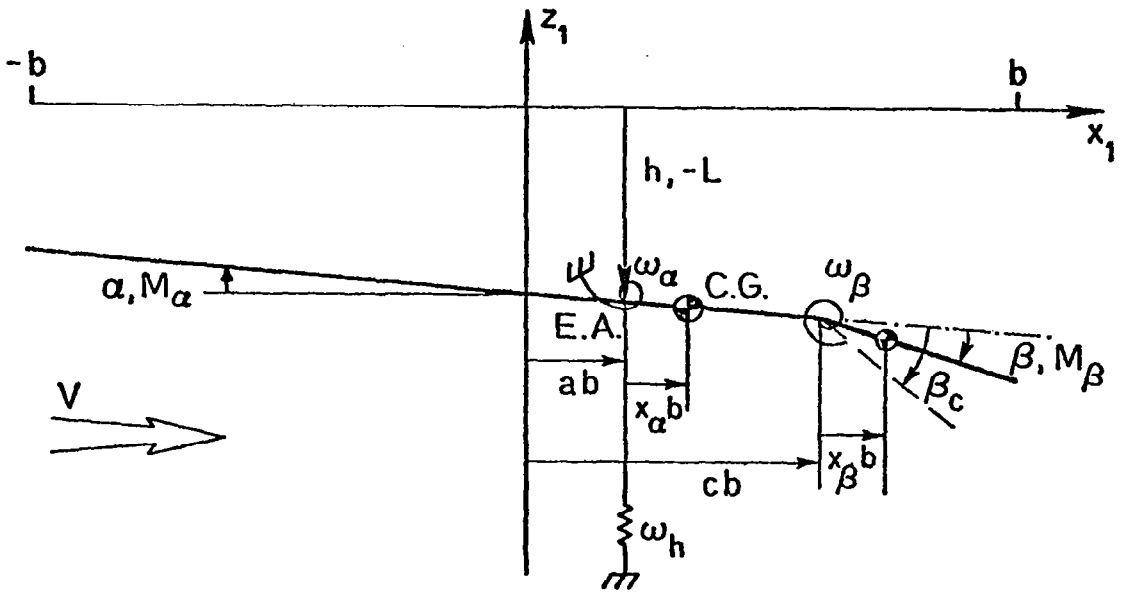

Figure 1: A typical section with aerodynamically unbalanced trailing-edge flap.

where s' is the non-dimensionalized Laplace variable $s' = sb/V$, and the aerodynamic influence coefficient matrix is

$$[A(s')] = 2b^2\left[[M_{nc}]s'^2 + \left[[B_{nc}]+C(s')\{R_1\}[S_2]\right]s' + [K_{nc}]+C(s')\{R_1\}[S_1]\right] \tag{2.11}$$

In this case, $C(s')$ is the generalized Theodorsen function

$$C(s') = \frac{K_1(s')}{K_0(s')+K_1(s')} \tag{2.12}$$

where K_n is a modified Bessel function of order n. The function $C(s')$ is analytic throughout the s' plane except for a branch point at the origin, which requires a branch cut along the negative real axis. The matrices of Eq. (2.11) and the series expansion of the Bessel functions are given in Appendix A. Equations (2.11) and (2.12) are identical to those given by Theodorsen [12] when s' is replaced by ik.

The two-dimensional oscillatory aerodynamic loads in subsonic flow were formulated by Timman and Van der Vooren [13] and are tabulated in the Manual of Aeroelasticity [43]. Vepa [24] and Edwards [20] generalized Possio's integral equation (2.7) for arbitrary motion in two-dimensional subsonic flow.

Finite Wings in Three-Dimensional Flow

Because a flying vehicle is a continuous elastic structure, the exact solution of the equations of motion requires infinite dimensional spaces.

Finite element modeling techniques [11] assume that the structure can be described by a finite number of degrees of freedom (DOF). A finite-element model of a complex wing structure may result in hundreds of DOF, for which as many natural frequencies and their associated mode shapes and generalized masses can be calculated. However, for global-structure aeroelastic analyses such as flutter and gust response, only a limited number of the lower frequency vibration modes is required [10].

The formulation of the preceding section is now generalized for finite wings in three-dimensional flow. The Laplace transform of the n DOF, open-loop, aeroelastic system equations of motion (for stability analysis) is

$$\left[[M_s]s^2 + [B_s]s + [K_s]\right]\{X(s)\} = q[A(s')]\{X(s)\} \tag{2.13}$$

Modal coordinates are used, which means that a discrete displacement is assumed to be a linear combination of a set of assumed modes,

$$x_d(x_1,y_1,t) = \sum_{i=1}^{n} x_{d,i}(t)\Psi_i(x_1,y_1) \tag{2.14}$$

When the assumed modes are dimensionless normal modes with natural frequencies $\omega_{n,i}$, and when modal-damping coupling is negligibly small, the structural matrices of Eq. (2.13) are diagonal and their elements are

$$M_{s,ii} = \iint_S m_s(x_1,y_1)\Psi_i^2(x_1,y_1)dx_1dy_1 \quad ; \tag{2.15}$$

$$B_{s,ii} = 2\zeta_i M_{s,ii}\omega_{n,i} \quad ;$$

and

$$K_{s,ii} = M_{s,ii}\omega_{n,i}^2$$

As stated previously, there are well-established numerical methods for solving Possio's integral equation (2.7) for oscillatory motion ($s' = ik$). Substituting $w' = w_j''\exp(i\omega t)$ and $z_a = b\Psi_j\exp(i\omega t)$ into Eq. (2.3) yields the non-dimensionalized oscillatory downwash due to motion (of amplitude b) in the j-th mode

$$\frac{w_j''(x_1,y_1;k)}{V} = ik\Psi_j + b\frac{\partial\Psi_j}{\partial x_1} \tag{2.16}$$

Solving Eq. (2.7) with the downwash Eq. (2.16) yields the j-th non-dimensionalized pressure mode $p_j''(x_1,y_1;k,M)/q$. The aerodynamic influence coefficient matrix for a given M is calculated by

$$A_{,ij}(ik) = -\frac{1}{b}\iint_S \frac{p_j''(x_1,y_1;k,M)}{q}\Psi_i(x_1,y_1)dx_1dy_1 \tag{2.17}$$

Extrapolation of the aerodynamic influence coefficients to the entire s' plane will be discussed later in this paper.

FLUTTER AND GUST RESPONSE ANALYSES

V-g Method for Flutter Analysis

The flutter boundary is the group of points of the flight envelope (in terms of airspeed and air density or altitude) at which the aeroelastic system is neutrally stable or, in other words, a disturbance results in simple harmonic oscillations. Thus, even though the computational tools were (and to a large extent still are) limited to oscillatory air loads, the flutter condition can still be found. The most popular technique for calculating the flutter conditions is the V-g method, originated by Smilg and Wasserman [17].

Because the effect of the structural damping terms in Eq. (2.13) is usually small, because it is difficult to calculate damping accurately, and because omitting damping is usually conservative, structural damping is neglected. For a simple harmonic motion of frequence ω, Eq. (2.13) can be written as

$$\left[[M_s] - \frac{1}{\omega^2}[K_s] + \frac{\rho b^2}{2k^2}[A(ik)]\right]\{X(ik)\} = \{0\} \tag{3.1}$$

A non-trivial solution of Eq. (3.1) with non-zero velocity and real ω is possible on the flutter boundary only. To find these conditions, an artificial structural damping g is introduced by replacing $1/\omega^2$ in Eq. (3.1) by

$$\Omega = (1+ig)/\omega^2 \tag{3.2}$$

Equation (3.1) becomes

$$[K_s]^{-1}\left[[M_s] + \frac{\rho b^2}{2k^2}[A(ik)]\right]\{X(ik)\} = \Omega\{X(ik)\} \qquad (3.3)$$

which is an eigenvalue problem to be solved for n eigenvalues Ω_i. Frequency of oscillations, air velocity and damping parameter are determined from each eigenvalue by

$$\omega_i=\sqrt{1/Re(\Omega_i)} \quad , \quad V_i=\omega_i b/k \quad , \quad g_i=Im(\Omega_i)/Re(\Omega_i) \qquad (3.4)$$

Given ρ and M, Eq. (3.3) is solved for several values of k. Curve fittings of the variations of g and ω with V yield the flutter velocity V_f and frequency ω_f at the point of g = 0, or when g equals some estimate of the damping present in the actual structure. The equivalent flutter speed V_{feq} is calculated by

$$V_{feq} = \sqrt{(\rho/\rho_{sl})}\, V_f \qquad (3.5)$$

The resulting $V_{feq}(M,\rho)$ does not necessarily match the actual equivalent velocity, $V_{eq} = \sqrt{\rho/\rho_{sl}}\, Ma_0$. To determine the actual flutter point for a given M, the flutter calculations are repeated iteratively with varying ρ until $V_{feq}(M,\rho)$ matches $V_{eq}(M,\rho)$. The group of actual flutter points, for various values of M, combine to form the flutter boundary.

An example of a flutter boundary and a practical flight envelope is given in Fig. 2. Three envelopes are plotted: the operating flight envelope which the airplane should not exceed in normal operation, (velocities up to V_{mo} and Mach numbers up to M_{mo}), the design envelope the airplane is designed for (maxium velocity V_d and maximum Mach numbers M_d),

and the safety margin envelope which is defined by aviation regulations (1.2 V_d and 1.2 M_d). On the Figure the h_{mo} and h_d refers to the maximum operational and design altitudes. Federal Aviation Administration (FAA) certification of a commercial transport airplane, for example, paragraph 25.629 of Ref. [29], requires that the unfailed airplane be designed to be flutter free to 1.2 times the design speed (V_d/M_d) and demonstrated by flight test to be flutter free up to V_d/M_d.

The graph of V_f should be out of the safety margin envelope for any weight loading and external store configuration. If not, as in the example of Fig. 2, the airplane should be placarded for lower V_{mo}/M_{mo} or modified structurally. Another alternative is to operate an active flutter suppression system which will drive the flutter boundary out of the safety margin envelope.

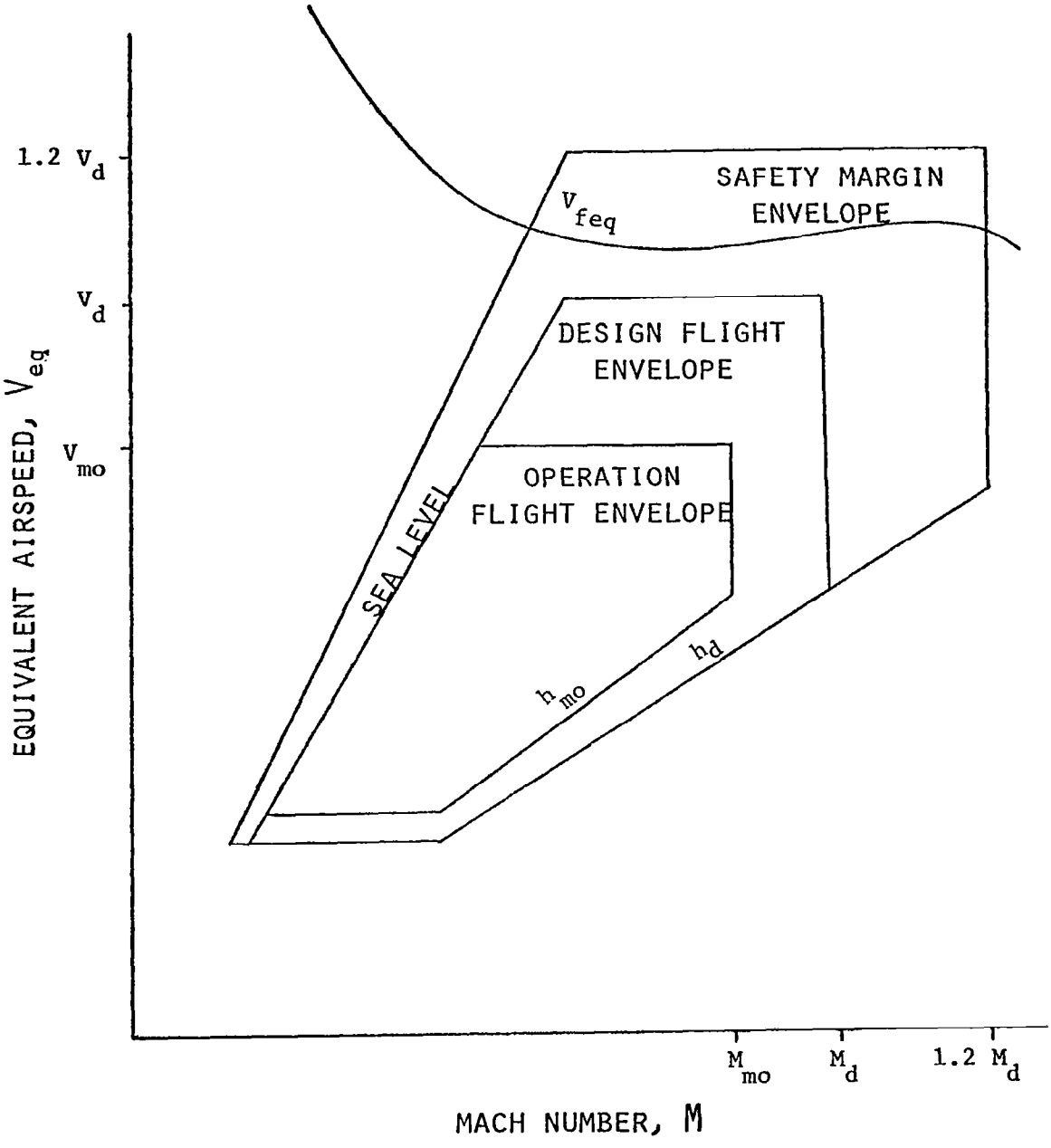

Figure 2: Example of flight envelopes and flutter boundary.

Root-Loci of the Aeroelastic Modes

The progress in developing analytical expressions and rational approximations for the aerodynamic influence coefficients for arbitrary motion now enable the use of root-loci analysis to determine the flutter boundary. The problem is to find the roots s_i which yield a non-trivial solution for Eq. (2.13), namely

$$\left|[M_s]s_i^2 + [B_s]s_i + [K_s] - q[A(s'_i)]\right| = 0 \qquad (3.6)$$

The main difficulty in solving Eq. (3.6) is in calculating $[A(s')]$. The solutions for $[A(s')]$ usually contain non-rational terms [19] and require lengthy calculations. Iterative procedures [19,20] are needed to solve Eq. (3.6) for s_i. Given M, Eq. (3.6) is solved for various q, and the root loci are plotted in the Laplace s plane. For stability, all roots should satisfy $Re(s_i) < 0$. The flutter dynamic pressure q_f is the q for which one of the roots is purely imaginary. The flutter frequency is

$$\omega_f = Im(s_i) \qquad \text{when} \qquad Re(s_i) = 0 \qquad (3.7)$$

In order to solve Eq. (3.6) by the methods of linear algebra, $[A(s')]$ has to be approximated by rational functions of s'. Rational approximations will be discussed later in this paper.

The root-loci method provides "correct" vibration frequencies and damping ratios at any flight condition, while the V-g method is correct on the flutter boundary only. Moreover, because ρ is not predetermined, the

root-loci flutter dynamic pressure represents an actual flight condition.

In design for active control of an aeroelastic system, the root-loci method is more advantageous because it fits modern control techniques, especially when rational approximations of the aerodynamic loads are used to construct finite order and constant coefficient system equations of motion, as will be discussed later.

Continuous Gust Response

An airplane traveling through the atmosphere encounters turbulence, which imposes gust loads on the structure. The turbulence and the associated gust response are defined in statistical terms, usually with the assumption that the process is stationary in time. A rigorous description of gust response analysis of a flexible airplane is given by Pratt [25]. A summary of the work on mathematical modeling of turbulence is given by Hinze [26].

The atmospheric gust waves can be described as a superposition of waves of all wavelengths. The basic assumptions regarding airplane-gust interaction are that the turbulence pattern does not change appreciably during the time the airplane passes through (known as Taylor's hypothesis) and that the gust field is uniform spanwise. The latter assumption is correct for most airplanes, except very large ones.

Consider an airplane flying horizontally with velocity V into a sinusoidal vertical gust of velocity amplitude w_g'' and wavelength λ. The gust downwash at a longitudinal station x_1 is

$$w_g = w_g'' \exp(-ikx_1/b) \exp(i\omega t) \tag{3.8}$$

where $\omega = 2\pi V/\lambda$ and $k = \omega b/V$

Substituting $w_g''\exp(-ikx_1/b)$ for w'' of Eq. (2.7) gives an integral equation for the nondimensionalized gust pressure difference p_g''/q. Substituting p_g''/q for p_j''/q in Eq. (2.17) gives the gust influence coefficients $A_{g,j}$. Adding the loads due to a sinusoidal vertical gust velocity of unit amplitude to Eq. (2.13) gives

$$\left[-\omega^2[M_s]+i\omega[B_s]+[K_s]-q[A(ik)]\right]\{X(i\omega)\} = (q/V)\{A_g(ik)\} \tag{3.9}$$

which is solved for the frequency response in generalized coordinates $X(i\omega)$. Any gust-induced structural frequency response $Z_d(i\omega)$ can be described as a linear combination of the displacement, velocity and acceleration frequency response in generalized coordinates.

$$Z_d(i\omega) = \left[[a_d]+i\omega[a_v]-\omega^2[a_o]\right]\{X(i\omega)\} \tag{3.10}$$

Before calculating the statistics of the gust response, the statistics of the atmospheric turbulence need to be known. The turbulence equations are very complicated, and closed-form solutions are available only in some specific cases. Isotropy and large Reynolds numbers are usually assumed for atmospheric turbulence. However, even with these assumptions the theoretical solutions are limited, and the mathematical models are based mainly on empirical and interpolation formulas.

The largest turbulence eddies (low wave numbers) are of permanent character. They contain relatively low energy per unit mass, but the energy dissipation by viscous effects is also very small. The larger eddies produce smaller ones through inertial interaction, thereby transferring energy to them such that the energy containment is increased with decreasing eddy sizes. At the same time, the viscosity effects become more and more important and, starting at some wave number, the energy decreases through dissipation.

The probability distribution of the gust velocity is assumed to be Gaussian, which implies that its statistical properties are defined by its power spectral density (PSD) $\Phi_{wg}(\omega)$. The PSD is a function of the coefficients of spatial longitudinal and vertical velocity correlation, $f(x_1)$ and $g(x_1)$, which are defined as

$$f(x_1) = \frac{\overline{u_g(0)u_g(x_1)}}{\sigma_{ug}^2} \quad , \quad g(x_1) = \frac{\overline{w_g(0)w_g(x_1)}}{\sigma_{wg}^2} \tag{3.11}$$

Isotropy implies $\sigma_{ug}^2 = \sigma_{wg}^2$ which defines the relations between the statistical properties of the longitudinal and vertical gust velocities. Based on experimental results, Dryden [27] suggested that $f(x_1)$ can be approximated, for $x_1 \geq 0$, by

$$f(x_1) = \exp(-x_1/L_g) \tag{3.12}$$

where L_g is a turbulence scale and depends on atmospheric conditions. As derived on page 174 of Ref. [26], the resulting PSD of the vertical gust velocity is

$$\Phi_{wg}(\omega) = \frac{\sigma_{wg}^2}{\pi} \frac{L_g}{V} \frac{1+3(\omega L_g/V)^2}{[1+(\omega L_g/V)^2]^2} \tag{3.13}$$

For high values of ω, $\Phi_{wg}(\omega)$ of Eq. (3.13) becomes proportional to $(\omega L_g/V)^{-2}$. Von Karman [28] indicated that it should be proportional to $(\omega L_g/V)^{-5/3}$ (known as the Kalmogoroff spectrum law) and gave an interpolation formula for the energy spectrum function which reads

$$\Phi_{wg}(\omega) = \frac{\sigma_{wg}^2}{\pi} \frac{L_g}{V} \frac{1+(8/3)(\omega/\omega_e)^2}{[1+(\omega/\omega_e)^2]^{11/6}} \tag{3.14}$$

where $$\omega_e = \sqrt{\pi} \frac{\Gamma(5/6)}{\Gamma(1/3)} \frac{V}{L_g} = 0.747 \frac{V}{L_g}$$

The PSD of the gust response is related to that of the gust velocity by

$$\Phi_{zd}(\omega) = |Z_d(i\omega)|^2 \Phi_{wg}(\omega) \tag{3.15}$$

The mean-square of the gust response is

$$\sigma_{zd}^2 = \int_0^\infty \Phi_{zd}(\omega) d\omega = \int_0^\infty |Z_d(i\omega)|^2 \Phi_{wg}(\omega) d\omega \tag{3.16}$$

A numerical example of gust response of the typical section of Fig. 1 in incompressible flow with V=275 b/sec was performed. (This is the first place in this work where new material appears.) The semichord b is use here and in later numerical examples as a length unit. The

frequency response was calculated using Eq. (3.9) with the structural parameters of Table 1, the gust loads of Eq. (A.11), and Dryden's PSD of Eq. (3.13), with $\sigma_{wg} = 1.(b/sec)^2$ and $Lg = 50b$. The resulting pitch angle frequency response and the pitch angle PSD are shown in Fig. 3.

TABLE 1

Three DOF typical section structural parameters

ω_h = 50 rad/sec	a = -0.4	x_α = 0.2
ω_α = 100 rad/sec	b = 1.	x_β = -0.025
ω_β = 300 rad/sec	c = 0.6	r_α^2 = 0.25
μ = 40		r_β^2 = 0.00625

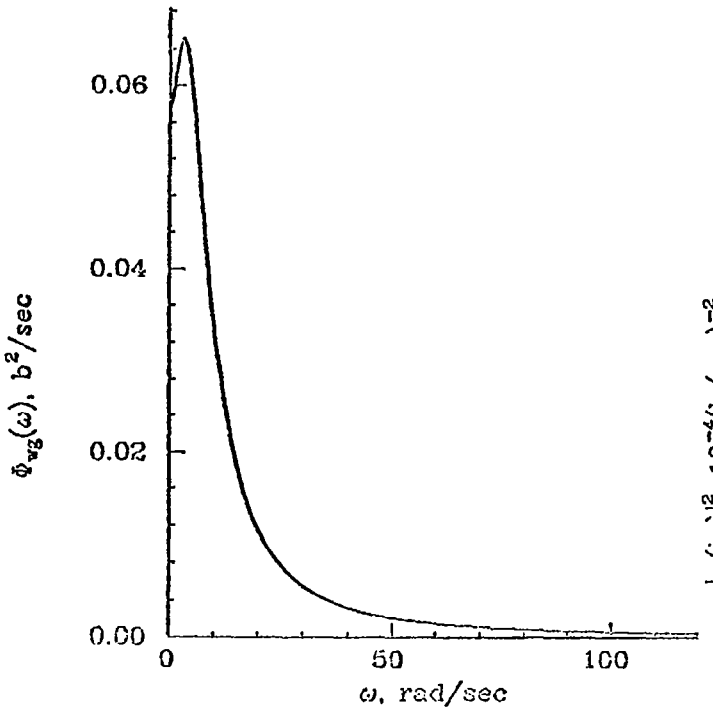

a) Input Gust Spectrum.

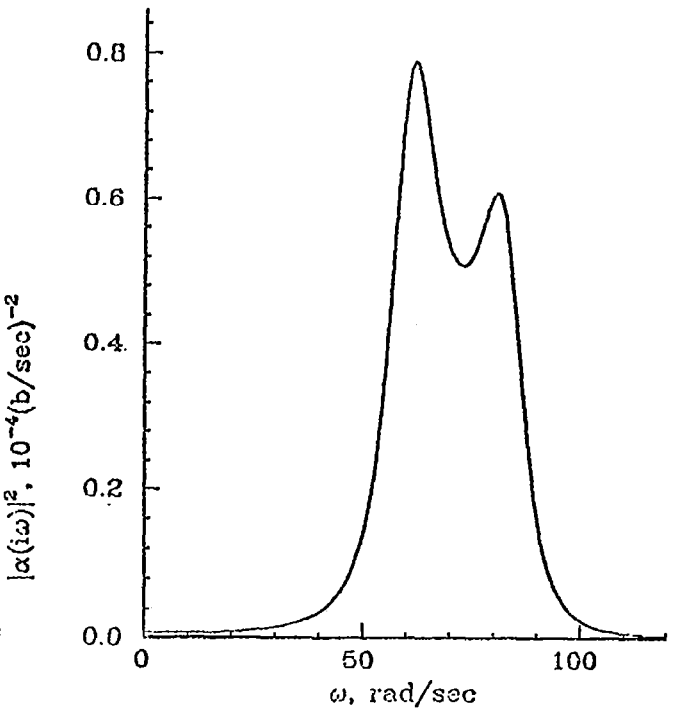

b) Pitch Angle Frequency Response.

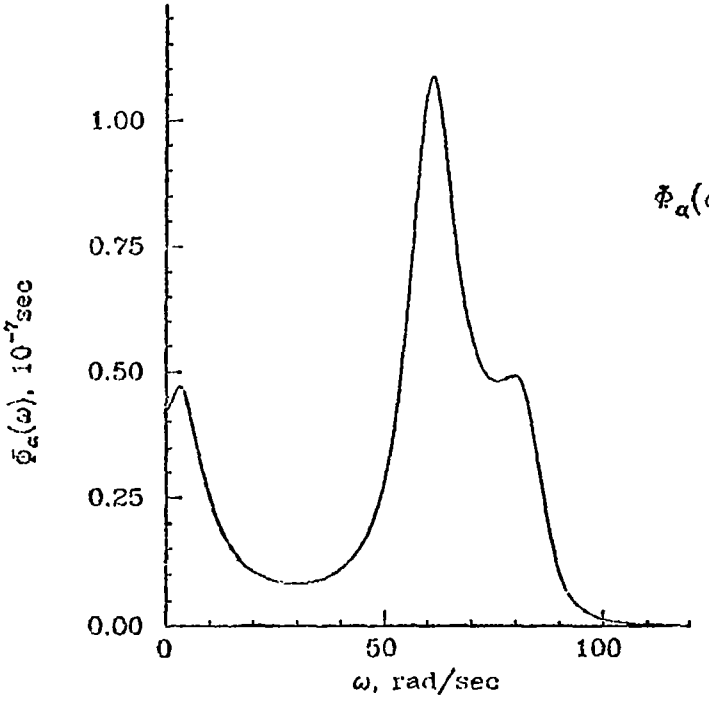

$$\Phi_\alpha(\omega) = |\alpha(i\omega)|^2 \Phi_{wg}$$

c) Pitch Angle Spectrum.

Figure 3: Dryden's gust PSD and gust response of a typical section in incompressible flow.

FINITE STATE-SPACE AEROELASTIC MODELING

As discussed previously, in order to solve aeroelastic equations by the methods of linear algebra, the aerodynamic influence coefficients have to be approximated by rational functions of s'. Such approximations enable finite, constant-coefficient, state-space modeling which best fits the formulation of modern control methods.

The form of an approximating function depends on the ranges of interest, required accuracy, exact data availability and approximation efficiency in later applications. Flutter reduced frequencies are usually within $k = 0.1$ to 0.5 (intermediate range). In stability and gust response analyses, however, lower reduced frequencies ($k \to 0$) are also important for the following reasons: (a) static instability (divergence) might occur, (b) the power spectral density of atmospheric gust velocities is much higher in the low frequency range, as shown in Fig. 3, and (c) rigid body modes may be included. When transient response is of concern, higher values of k (or s') are required. This range is beyond the scope of this study.

As discussed in the preceding section, three-dimensional aerodynamic routines are well developed for oscillatory motion only (along the imaginary axis of the s plane). Rational approximations are designed

to fit these data and are then extrapolated to the entire s plane by replacing ik by s'. The adequacy of this extrapolation will be demonstrated later in this section. The higher the order of the approximation (the number of denominator roots), the more accurate is the approximation, but the resulting state-space model is also of higher order (less efficiency). The numerical examples in this and following sections consist of the aeroelastic systems given in Table 2,

TABLE 2

Aeroelastic systems for numerical examples

	Typical section	Typical section	Research wing
Figure	1	1	4
Mach number	0.	0.7	0.9
DOF	3: h,α,β	3: h,α,β	4: three wing modes and one control surface deflection mode
Structural properties	Table 1, Eq. (2.9)	a=-0.5 , b=1. c=0.6	Abel [6]
Aerodynamic data sources	Eq. (2.11), Appendix A	Manual of aeroelasticity [44]	Doublet lattice method [15], supplied by Irving Abel of NASA-Langley and normalized for unit generalized mass
Tabulated k values	0., 0.1, 0.15, 0.25, 0.3, 0.5, 1.0, 2.0	0., 0.06, 0.1, 0.16, 0.22 0.26, 0.3, 0.4, 0.5, 0.64, 0.8, 1.0	0., 0.1, 0.3, 0.5, 0.7, 0.9, 1.3

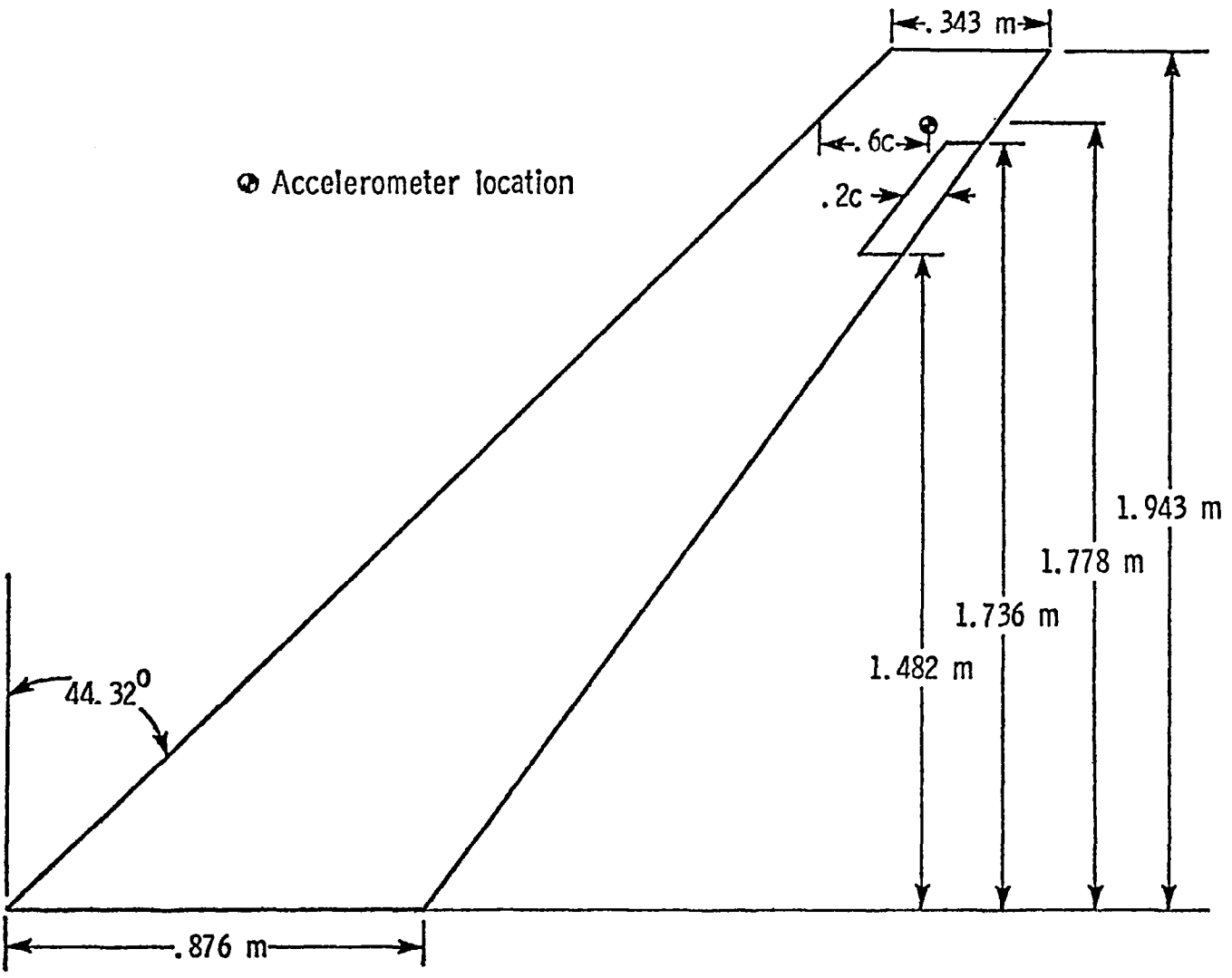

Figure 4: Research wing geometry (taken from Ref. [6]).

Linear Least-Squares Solution

A basic tool in rational approximations is the least-squares technique [45]. Given l_e data points, the problem is to find $[X_e]$ which approximates the solution of the linear system

$$\underset{n_e x m_e}{[A_l]} \; \underset{m_e x p_e}{[X_e]} \simeq \underset{n_e x p_e}{[B_l]} \qquad l=1,l_e \tag{4.1}$$

where $[A_l]$ and $[B_l]$ are functions of the tabulated data at each point. A "best fit" is obtained by minimizing the cost function

$$J_e = \sum_{l=1}^{l_e} \sum_{j=1}^{p_e} \sum_{i=1}^{n_e} \varepsilon_{l,ij}^2 \tag{4.2}$$

where $\varepsilon_{l,ij} = [A_{l,i}]\{X_{e,j}\} - B_{l,ij}$

The least-squares criterion is satisfied by the solution of the normal equations of the least-squares problem:

$$\left(\sum_{l=1}^{l_e} [A_l]^t [A_l] \right) [X_e] = \sum_{l=1}^{l_e} [A_l]^t [B_l] \tag{4.3}$$

When applied to approximating aerodynamic data, an index l refers to a known reduced frequency k_l. The desired accuracy in different frequency regions can be controlled by (a) spacing the data points, (b) weighting the data by multiplying $[A_l]$ and $[B_l]$ by different parameters for different l indices, and (c) requiring the approximation to match the data at some points. Matching can be done by either constraining some of the free parameters (as will be shown later) or applying large weights to the data of these points.

The matrix Padé method and the minimum-state method lead to least-squares problems which involve different terms of the data matrices simultaneously. The modal coordinates on which the aerodynamic data are based should be normalized such that the different terms are of comparable order of magnitude.

Term-by-Term Padé Approximants

R. T. Jones [21] first introduced the use of rational Laplace transfer functions to approximate incompressible unsteady loads. Based on an exponential approximation of Wagner's indicial loading function (loading due to a step change in angle of attack), Jones' approximation of the generalized Theodorsen function reads

$$C(s') \simeq 0.5 + \frac{0.0075}{s'+0.0455} + \frac{0.10055}{s'+0.3} \tag{4.4}$$

The branch cut along the negative real axis required for the exact function, Eq. (2.12), is replaced by two poles there. Edwards [18] used Jones' approximation to model the typical section with a state-space model of order 8 (six structural and two augmented states).

In a more general aeroelastic system, unlike the incompressible, two-dimensional aerodynamics (Eq. (2.11)) case, there is no longer a single non-rational function which can be factored out of the influence coefficient matrices. This complication led to a Padé approximant technique [3,24], in which each term of the influence coefficient matrix is approximated by a different ration of polynomials in s'.

In a Padé approximant of order m, a least-squares technique is used to find the numerator and denominator polynomials which best fit tabulated influence coefficients for oscillatory motion. Since each approximation root adds one state to the equation of motion, the dimension of an n DOF model becomes $2n+mn^2$. In a realistic problem, the contributions of some of these roots are negligible and are omitted. In the design problem of Ref. [3], for instance, a system of 27 structural modes was analyed with a mathematical model of the order of 200.

Roger's Approximation

Roger [23] realized that the aerodynamic influence coefficients may be approximated more efficiently by using common denominator roots. His approximation is

$$[A_{ap}]_{nxn} = [P_0]+[P_1]s'+[P_2]s'^2 + \sum_{j=3}^{N} \frac{[P_j]s'}{(s'+\gamma_{j-2})} \tag{4.5}$$

where the values of γ_{j-2} are selected to be in the reduced frequency range of interest. The real coefficient matrices $[P_j]$ are found by setting $s' = ik$ and using a least-squares technique for a term-by-term fitting of tabulated oscillatory influence coefficient matrices $[A(ik_l)] = [F(k_l)] + i[G(k_l)]$ for various l indices. The parameters of the normal least-squares equations (4.3) for the ij-th terms are

$$[A_l] = \begin{bmatrix} 1 & 0 & -k_l^2 & \frac{k_l^2}{k_l^2+\gamma_1^2} & \cdots & \frac{k_l^2}{k_l^2+\gamma_{N-2}^2} \\ 0 & k_l & 0 & \frac{k_l\gamma_1}{k_l^2+\gamma_1^2} & \cdots & \frac{k_l\gamma_{N-2}}{k_l^2+\gamma_{N-2}^2} \end{bmatrix}$$

$$[B_1] = \begin{Bmatrix} F_{,ij}(k_1) \\ \\ G_{,ij}(k_1) \end{Bmatrix} \quad \text{and} \quad [X_a] = \begin{Bmatrix} P_{0,ij} \\ \bullet \\ \bullet \\ P_{N,ij} \end{Bmatrix} \tag{4.6}$$

An augmented state vector is defined by

$$\underset{nx1}{\{X_{ai}(s)\}} = \frac{s}{s+(V/b)\gamma_{i-2}}\{X(s)\} \tag{4.7}$$

Equation (2.13) can now be re-transformed to a state-space matrix equation of motion for stability analysis

$$\begin{Bmatrix} \dot{x} \\ \ddot{x} \\ \dot{x}_{a3} \\ \bullet \\ \bullet \\ \bullet \\ x_{aN} \end{Bmatrix} = \begin{bmatrix} 0 & [I] & 0 & \bullet\bullet\bullet & 0 \\ -[M]^{-1}[K] & -[M]^{-1}[B] & [M]^{-1}[P_3] & \bullet\bullet\bullet & [M]^{-1}[P_N] \\ 0 & [I] & -(V/b)\gamma_1[I] & & 0 \\ \bullet & \bullet & & \bullet & \\ \bullet & \bullet & & \bullet & \\ \bullet & \bullet & & \bullet & \\ 0 & [I] & 0 & & -(V/b)\gamma_{N-2}[I] \end{bmatrix} \begin{Bmatrix} x \\ \dot{x} \\ x_{a3} \\ \bullet \\ \bullet \\ \bullet \\ x_{aN} \end{Bmatrix} \tag{4.8}$$

where $[M] = [M_s] - \frac{1}{2}\rho b^2[P_2]$

$[B] = [B_s] - \frac{1}{2}\rho bV[P_1]$

and $[K] = [K_s] - \frac{1}{2}\rho V^2[P_0]$

The state-space model is of the order of Nn. Most applications (such as Refs. [6] and [46]) used N = 6. Roger's method was applied to approximate the aerodynamic data of the research wing of Table 2. A best fit with N = 3, 4, 5 and 6 was obtained with $\gamma_1 = 0.2$, $\gamma_2 = 0.4$, $\gamma_3 =$

0.6 and $\gamma_4 = 0.8$. The results for uniform weighting are typified by the curve fittings of $A_{1,1}(ik)$ and $A_{2,2}(ik)$, which are shown in Fig. 5. Two other cases were analyzed, one in which the approximation is required to match the data at k = 0.3 and one in which the matching requirement is for both k = 0 and k = 0.3. The matching requirement is imposed by assigning large weights to the relevant data points. The total squared errors for the different cases is given in Table 3.

TABLE 3

Roger's approximation errors and aerodynamic roots

N	Sum of squared errors, m^2			Aerodynamic roots ($-\gamma_i$)
	Uniform weighting	Match k=0.3	Match k=0. and 0.3	
3	.3406	.4463	2.5664	-.2
4	.1128	.1485	.1650	-.2, -.4
5	.0270	.0437	.0483	-.2, -.4, -.6
6	.0065	.0079	.0087	-.2, -.4, -.6, -.8

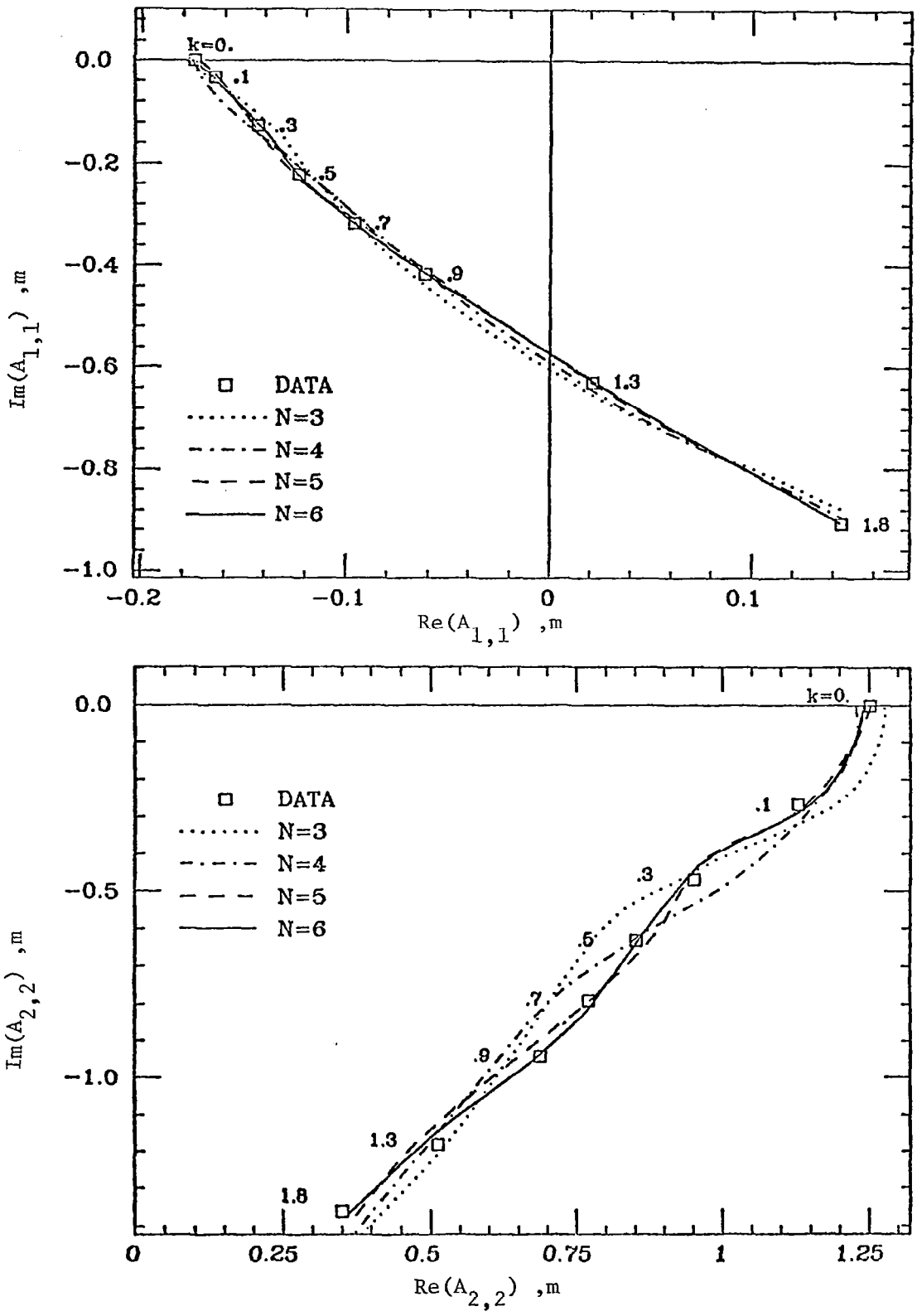

Figure 5: Roger's approximation of $A_{1,1}$ and $A_{2,2}$ of the research wing at M = 0.9.

Matrix Padé Approximations

The matrix Padé approximant technique was introduced by Vepa [24], was modified by Edwards [20] and is further modified here. The approximant is

$$[A_{ap}] = \left(s'[I]-[R]\right)^{-1}\left([P_1]s'^2+[P_2]s'+[P_3]\right) \tag{4.9}$$

The data used to determine the approximant consist of tabulated steady-state influence coefficients $[F(0)]$ and oscillatory influence coefficients $[A(ik_1)] = [F(k_1)] + i[G(k_1)]$ for various l indices. A requirement of matching the steady-state aerodynamics yields

$$[P_3] = -[R][F(0)] \tag{4.10}$$

$[P_1]$ and $[P_2]$ are related to $[R]$ by

$$[P_1] = [R]([F(k_{f1})]-[F(0)])/k_{f1}^2+[G(k_{f1})]/k_{f1} \tag{4.11a}$$

and

$$[P_2] = [F(k_{f2})]-[R][G(k_{f2})]/k_{f2} \tag{4.11b}$$

where k_{f1} and k_{f2} are selected from the tabulated k values. Equations (4.11a) and (4.11b) are only approximations at other k_l values, for which

$$[A_{1,l}]^t[R]^t \simeq [B_{1,l}]^t \tag{4.12a}$$

and

$$[A_{2,l}]^t[R]^t \simeq [B_{2,l}]^t \tag{4.12b}$$

where $[A_{1,l}] = ([F(k_l)]-[F(0)])/k_l^2 - ([F(k_{r1})]-[F(0)])/k_{r1}^2$

$$[A_{2,1}] = [G(k_1)]/k_1 - [G(k_{r2})]/k_{r2}$$

$$[B_{1,1}] = [G(k_{r1})]/k_{r1} - [G(k_1)]/k_1$$

and $$[B_{2,1}] = [F(k_1)] - [F(k_{r2})]$$

where k_{r1} and k_{r2} are selected from the tabulated k_1 values.

Edwards [20] used $k_{f1} = k_{f2} = k_f$, which causes the approximant to be exact at k_f. He chose $k_{r1} \to \infty$ which yields $([F(k_{r1})]-[F(0)])/k_{r1}^2 \to 0$ and $[G(k_{r1})]/k_{r1} \to [Q_{pt}]$. He also used Eq. (4.12a) only to construct a matrix least-squares problem to be solved for $[R]^t$.

The matrix Padé approximation is improved when both Eqs. (4.12a) and (4.12b) are used for least-squares fitting, which yields Eq. (4.3) with

$$[A_1] = \begin{bmatrix} [A_{1,1}]^t \\ [A_{2,1}]^t \end{bmatrix} \quad , \quad [B_1] = \begin{bmatrix} [B_{1,1}]^t \\ [B_{2,1}]^t \end{bmatrix} \quad , \quad [X_e] = [R]^t \qquad (4.13)$$

The matrix Padé technique was applied to the research wing of Table 2 (with the wing modes only) for different k_f and k_r values. The sum of the squared errors and the aerodynamic roots (eigenvalues of [R]) for the different cases are given in Table 4.

Best overall accuracy is obtained by taking $k_{f1} = k_{r1} = \max(k_1)$ and $k_{f2} = k_{r2} = k_1$ at which accuracy is most important (case 1 of Table 4). The comparison with other methods is shown in Fig. 8. To yield the approximation to match the data at k = 0.3, one can set $k_{f1} = k_{f2} = 0.3$ (rather than $= k_{r1}$), but there is a penalty in deteriorating accuracy at

TABLE 4

Matrix Padé approximation errors and aerodynamic roots

Case	k_{f1}	k_{f2}	k_{r1}	k_{r2}	Sum of squared errors, m^2	Aerodynamic roots
1	1.8	0.3	1.8	0.3	.183	-.136, -.946, -1.928
2	0.3	0.3	1.8	1.8	.703	-.138,-1.584, -2.474
3	0.3	0.3	1.8	0.3	.701	-.136, -.946, -1.928
4	0.3	0.3	0.3	0.3	.974	-.141, -.961, -1.632

higher reduced frequencies (case 3 of Table 4). The matrix Padé technique yields a state-space model of order 3n (Ref. [19]), which reads

$$\begin{Bmatrix} \dot{x} \\ \ddot{x} \\ \dot{x}_a \end{Bmatrix} = \begin{bmatrix} 0 & [I] & 0 \\ -[M_s]^{-1}[K_s] & -[M_s]^{-1}[B_s] & q[M_s]^{-1} \\ (V/b)[P_3]-[P_1']{}[K_s] & [P_2]-[P_1']{}[B_s] & (V/b)[R]+q[P_1'] \end{bmatrix} \begin{Bmatrix} x \\ \dot{x} \\ x_a \end{Bmatrix} \quad (4.14)$$

where $[P_1'] = (b/V)[P_1][M_s]^{-1}$

Minimum-State Method

Roger's method and the matrix Padé method provide straightforward linear least-squares solutions. Inspection

of the associated state-space equations (4.8) and (4.14), however, suggests that their efficiency, in terms of number of augmented states per given accuracy in approximating the aerodynamic influence coefficients, can be improved.

Another approach taken here involves analyzing the state-space equations first. A general state-space representation of an n DOF aeroelastic system with m aerodynamic augmented states for stability analysis reads:

$$\begin{Bmatrix} \dot{x} \\ \ddot{x} \\ \dot{x}_{a1} \end{Bmatrix} = \begin{bmatrix} 0 & [I] & 0 \\ [K_1] & [B_1] & [D_1] \\ [E_1] & [E_2] & [R_1] \end{bmatrix} \begin{Bmatrix} x \\ \dot{x} \\ x_{a1} \end{Bmatrix} \quad \begin{matrix} n \\ n \\ m \end{matrix} \tag{4.15}$$

The target now is to define the matrices of Eq. (4.15) in a way that is most convenient for the aerodynamic approximation, and without reducing the generality of Eq. (4.15). The structural states $\{x\}$ and $\{\dot{x}\}$ represent the physical and measurable motion of the structure, in terms of which the structural properties and the tabulated aerodynamic data are given. The aerodynamic augmented states will now be redefined to reduce the number of free parameters in Eq. (4.15), without changing the structural states.

The eigenvalues of $[R_1]$ represent the aerodynamic time lags. When these eigenvalues are constrained to be real and negative with linearly independent eigenvectors, there exists a similarity transformation matrix [T] (Ref. [47]) such that

$$[R] = [T]^{-1}[R_1][T] \tag{4.16}$$

where $[R]$ is diagonal with the same eigenvalues as $[R_1]$. By defining a new augmented state vector,

$$\{x_{a2}\} = [T]^{-1}\{x_{a1}\}, \tag{4.17}$$

equation (4.15) becomes

$$\begin{Bmatrix} \dot{x} \\ \ddot{x} \\ \dot{x}_{a2} \end{Bmatrix} = \begin{bmatrix} 0 & [I] & 0 \\ [K_1] & [B_1] & [D_2] \\ [E_3] & [E_4] & [R] \end{bmatrix} \begin{Bmatrix} x \\ \dot{x} \\ x_{a2} \end{Bmatrix} \tag{4.18}$$

where $[D_2] = [D_1][T]$, $[E_3] = [T]^{-1}[E_1]$

and $[E_4] = [T]^{-1}[E_2]$.

A new augmented state vector is now defined as

$$\{x_a\} = \{x_{a2}\} + [R]^{-1}[E_3]\{x\}. \tag{4.19}$$

Differentiating Eq. (4.19) and using the last row of Eq. (4.18) gives

$$\{\dot{x}_a\} = [E_3]\{x\} + \left([E_4]+[R]^{-1}[E_3]\right)\{\dot{x}\} + [R]\{x_{a2}\}. \tag{4.20}$$

Substituting Eq. (4.19) for $\{x_{a2}\}$ gives

$$\{\dot{x}_a\} = \left([E_4]+[R]^{-1}[E_3]\right)\{\dot{x}\} + [R]\{x_a\}. \tag{4.21}$$

Using Eqs. (4.19) and (4.21) to eliminate $\{x_{a2}\}$ from Eq. (4.18) gives

$$\begin{Bmatrix} \dot{x} \\ \ddot{x} \\ \dot{x}_a \end{Bmatrix} = \begin{bmatrix} 0 & [I] & 0 \\ [K_2] & [B_1] & [D_2] \\ 0 & [E] & [R] \end{bmatrix} \begin{Bmatrix} x \\ \dot{x} \\ x_a \end{Bmatrix} \tag{4.22}$$

where $[K_2] = [K_1] - [D_2]^{-1}[E_3]$

and $[E] = [E_4] + [R]^{-1}[E_3]$

The matrices of the second row of Eq. (4.22) are now defined such that the structural properties are separated from the aerodynamic ones. This yields

$$\begin{Bmatrix} \dot{x} \\ \ddot{x} \\ \dot{x}_a \end{Bmatrix} = \begin{bmatrix} 0 & [I] & 0 \\ -[M_s+M_a]^{-1}[K_s+K_a] & -[M_s+M_a]^{-1}[B_s+B_a] & [M_s+M_a]^{-1}[D] \\ 0 & [E] & [R] \end{bmatrix} \begin{Bmatrix} x \\ \dot{x} \\ x_a \end{Bmatrix} \tag{4.23}$$

Comparing Eq. (4.23) with Eq. (2.13) shows that the aerodynamic influence coefficient matrix is approximated by

$$\underset{nxn}{[A_{ap}(s')]} = [P_1]s'^2 + [P_2]s' + [P_3] + \underset{nxm}{[D']}\left(\underset{mxm}{s'[I]-[R']}\right)^{-1}\underset{mxn}{[E']}s' \tag{4.24}$$

where the aerodynamic parameters of Eq. (4.23) are related to those of Eq. (4.24) by

$$[M_a] = -\tfrac{1}{2}\rho b^2[P_1] \quad , \quad [B_a] = -\tfrac{1}{2}\rho bV[P_2] \quad ,$$

$$[K_a] = -\tfrac{1}{2}\rho V^2[P_3] \quad , \quad [D] = \tfrac{1}{2}\rho V^2[D'] \quad , \tag{4.25}$$

$$[E] = [E'] \quad , \quad [R] = (V/b)[R'] \quad , \quad s = s'V/b$$

The approximation of Eq. (4.24) is constrained to match the influence coefficients for k = 0 and k = k_f. Thus,

$$[P_1] = ([F(0)]-[F(k_f)])/k_f^2+[D'](k_f^2[I]+[R']^2)^{-1}[E'] \quad (4.26a)$$

$$[P_2] = [G(k_f)]/k_f+[D'](k_f^2[I]+[R']^2)^{-1}[R'][E'] \quad (4.26b)$$

and

$$[P_3] = [F(0)] \quad (4.26c)$$

For the other tabulated reduced frequencies, Eqs. (4.26a) and (4.26b) become approximations. Thus one obtains

$$[D'][C(R',k_1)][E] \cong ([F(k_1)]-[F(0)])/k_1^2-([F(k_f)]-[F(0)])/k_f^2 \quad (4.27a)$$

and $$[D'][C(R',k_1)][R'][E'] \cong [G(k_f)]/k_f - [G(k_1)]/k_1 \quad (4.27b)$$

where $$[C(R',k_1)]=(k_1^2[I]+[R']^2)^{-1}-(k_f^2[I]+[R']^2)^{-1}$$

Equations (4.27a) and (4.27b) constitute a non-linear least-squares problem to be solved for [D'], [R'] and [E']. The real part of the tabulated data is weighted in Eq. (4.27a) by $1/k_1^2$ and the imaginary part is weighted in Eq. (4.27b) by $1/k_1$. These are only examples which illustrate weighting the data for higher accuracy at low reduced frequencies. With uniform weighting Eq. (4.27) becomes

$$k_1^2[D'][C(R',k_1)][E'] \cong [F(k_1)]-[F(0)]-([F(k_f)]-[F(0)])(k_1/k_f)^2 \quad (4.28a)$$

and $$k_1[D'][C(R',k_1)][R'][E'] \cong [G(k_f)]k_1/k_f-[G(k_1)] \quad (4.28b)$$

The minimum-state procedure goes as follows:

1. Set an initial number of augmented states m.

2. Set an initial diagonal $[R']$ with distinct negative elements.

3. Set an initial $[D']$ with rank $[D'] = \min(m,n)$.

4. Form a linear least-squares problem to be solved for $[E']$. For the uniform weighting of Eq. (4.28), the parameters of the normal equations (4.3) are

$$[X_e] = [E'] \quad , \quad [A_1] = \begin{bmatrix} k_1^2[D'][C(R',k_1)] \\ k_1[D'][C(R',k_1)][R'] \end{bmatrix}$$

$$\text{and} \quad [B_1] = \begin{bmatrix} [F(k_1)]-[F(0)]-(F(k_f)]-[F(0)])(k_1/k_f)^2 \\ [G(k_f)]k_1/k_f-[G(k_1)] \end{bmatrix} \tag{4.29}$$

The summation is done over all the data points except those corresponding to $k = 0$ and $k = k_f$.

5. Form a linear least-squares problem to be solved for $[D']$. The parameters of Eq. (4.3) are:

$$[X_e] = [D']^t \quad , \quad [A_1] = \begin{bmatrix} k_1^2[E']^t[C(R',k_1)] \\ k_1[E']^t[R'][C(R',k_1)] \end{bmatrix}$$

$$\text{and } [B_1] = \begin{bmatrix} [F(k_1)]^t-[F(0)]^t-([F(k_f)]-[F(0)])^t(k_1/k_f)^2 \\ [G(k_f)]^tk_1/k_f-[G(k_1)]^t \end{bmatrix} \tag{4.30}$$

6. Calculate the least-squares performance index J_e by Eq. (4.2).

7. Repeat steps 4 to 6 to convergence.

8. Use a minimization procedure to modify [R′]. The procedure used in this work is based on a modification of Davidon's method [37] as given by Stewart [39].

9. Repeat steps 4 through 8 until the performance index converges to a global minimum.

10. Calculate the approximant of Eq. (4.24) for the tabulated reduced frequencies and compare with the tabulated data.

11. If the accuracy of the approximant is insufficient in a limited frequency range only, try changing the weighting of the data. If the insufficient accuracy is related to a specific mode, try changing the modal normalization to increase the weight of the associated terms. Repeat steps 4 through 10.

12. If the accuracy of the approximant is still not satisfactory, increase m and repeat steps 2 through 11.

Numerical Examples Employing the Minimum-State Method

The minimum-state procedure is first applied to the typical section of Table 2 in incompressible flow. The tabulated aerodynamic influence coefficients were calculated for pure imaginary s′ values, using Theodorsen's formulation as given in Appendix A. The matching reduced frequency is $k_f = 0.25$ and the least-squares weighting is that of Eq. (4.27). The results are typified by $A_{1,2}$ which is, divided by $-2b^2$,

the unsteady lift-curve slope C_{ℓ_α}. A comparison between C_{ℓ_α} obtained from Theodorsen, Jones' approximation (Eq. (4.4)), and the minimum-state method of order 2 (Eq. (4.24)), is given in Fig. 6 for various values of $s' = r \exp(i\theta)$.

The optimized aerodynamic roots obtained by the minimum-state method are -0.04746 and -0.2285, while those of R. T. Jones are -0.0455 and -0.3. While both approximations yield state-space equations of the same order (8), the minimum-state procedure is seen to yield a better approximation in the entire range of interest $|r| < 1.$ and $60^0 < \theta < 120^0$. Both approximations deteriorate as the branch cut along the negative real axis is approached.

Although good accuracy is shown in this example for a wide range off the imaginary axis, one should not conclude that a rational approximation, based only on oscillatory aerodynamic data, will always have similar accuracy in the entire s plane. As indicated by H. Ashley and W.N. Boyd, in a paper presented at Colloquium Honoring Hans Georg Kussner (1980), serious inadequacies might occur when the approximations are applied to three-dimensional wings in compressible flow.

The minimum-state procedure, with the least-squares weighting of Eq. (4.27) and $k_f = 0.26$, was also applied to the typical section of Table 2 in subsonic flow of $M = 0.7$. The tabulated aerodynamic matrices were taken from Ref. [44]. The sum of the squared errors and the aerodynamic roots for various approximation orders are given in Table 5. The approximants of order 1, 2, 4, and 6 are compared to the tabulated oscillatory C_{ℓ_α} in Fig. 7. The first-order approximation is quite poor. Starting with $m = 2$, it is up to the designer to make the trade-off between the approximation accuracy and the order of the resulting model.

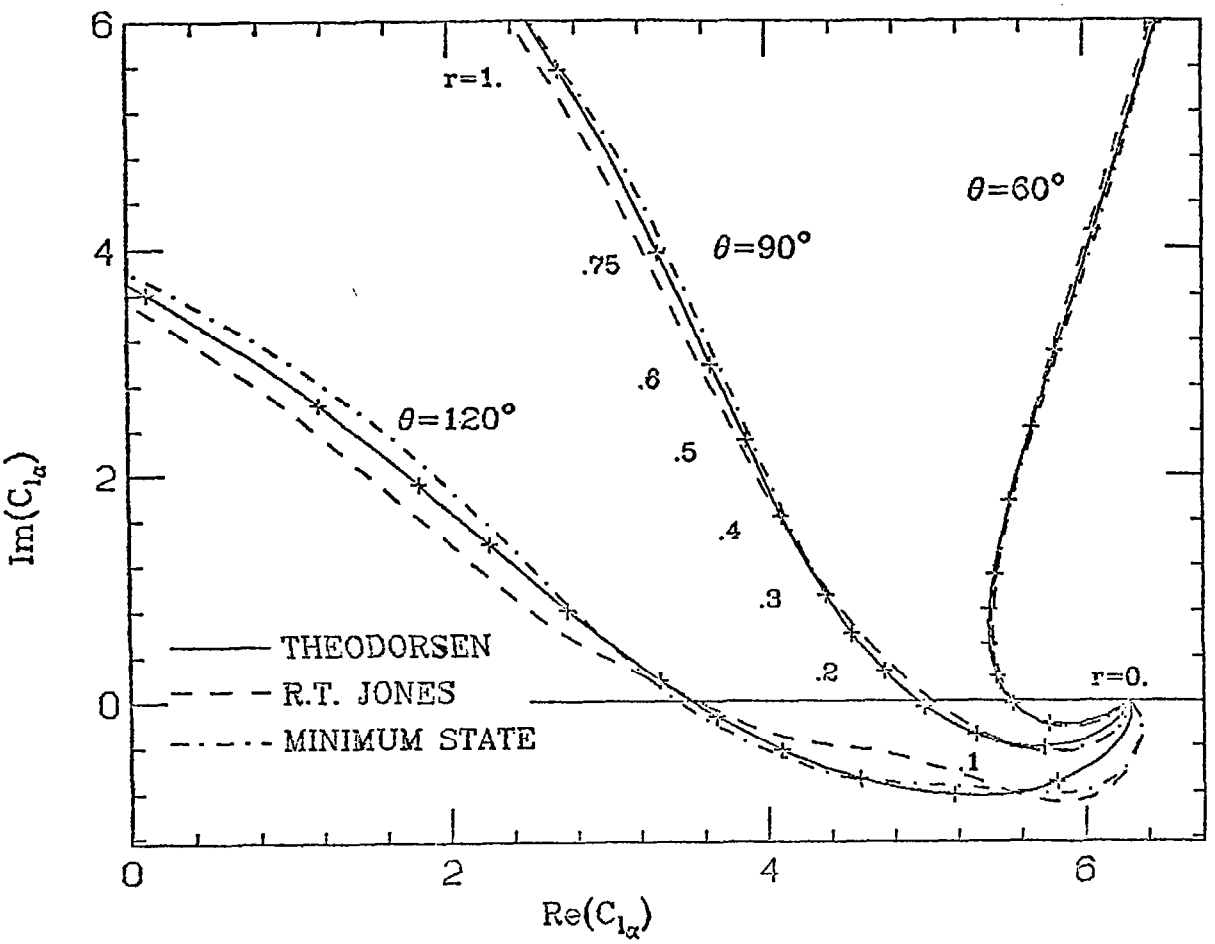

Note: The values of r at the +'s along the curves for θ = 60° and 120° are the same as for θ = 90°.

Figure 6: Rational approximations of C_{ℓ_α} of a typical section at M=0 as a function of $s' = r \exp(i\theta)$.

TABLE 5

Minimum-state approximation errors, typical section at M=0.7

Approximation order (m)	Aerodynamic roots (diagonal of [R'])	Sum of squared errors, b^4
1	-.0600	1791.0
2	-.0301,-.1248	73.3
3	-.0286,-.1214,-.9389	36.0
4	-.0281,-.1214,-.9389,-3.4279	27.3
5	-.0260,-.0594,-.1501,-.7913,-1.969	9.7
6	-.0099,-.0483,-.1424,-.2727,-1.0241,-1.5107	5.6

The last example chosen was the research wing of Table 2. The minimum-state procedure, with uniform data weighting (Eq. (4.28)) and k_f = 0.3, gave satisfactory results with four aerodynamic roots (m = 4). The optimized aerodynamic roots are -0.181, -0.384, -1.496 and -2.033. The sum of the square errors is 0.0332. This error is comparable to the errors obtained with Roger's approximation with N=5 (Table 3). However, while the minimum-state approximation with m=4 requires four augmented states in the aeroelastic model, Roger's approximation with N=5 requires 12 augmented states.

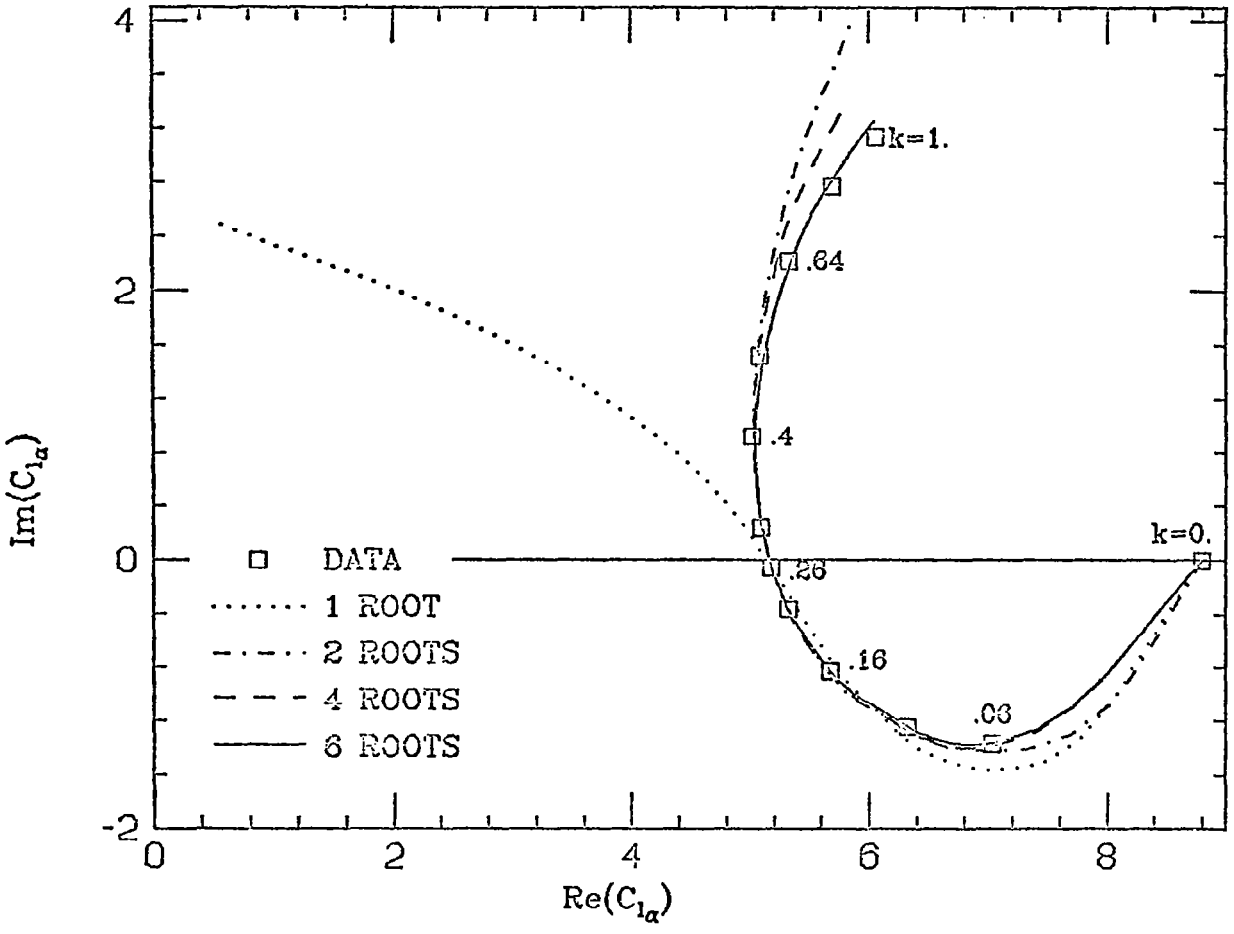

Figure 7: Minimum-state approximation of C_{ℓ_α} of a typical section at M=0.7.

The minimum-state error is much smaller than the matrix Padé errors of Table 4. Curve fittings for selected aerodynamic terms using Roger's approximation with N=6, the modified matrix Padé approximant (case 1 of Table 4) and the minimum-state approximation are shown in Fig. 8. The minimum-state approximations are within 3% of the data in the low frequency range ($k < 0.5$) and 5% in the higher range.

The minimum-state approximations will be used in the numerical examples discussed in the following section.

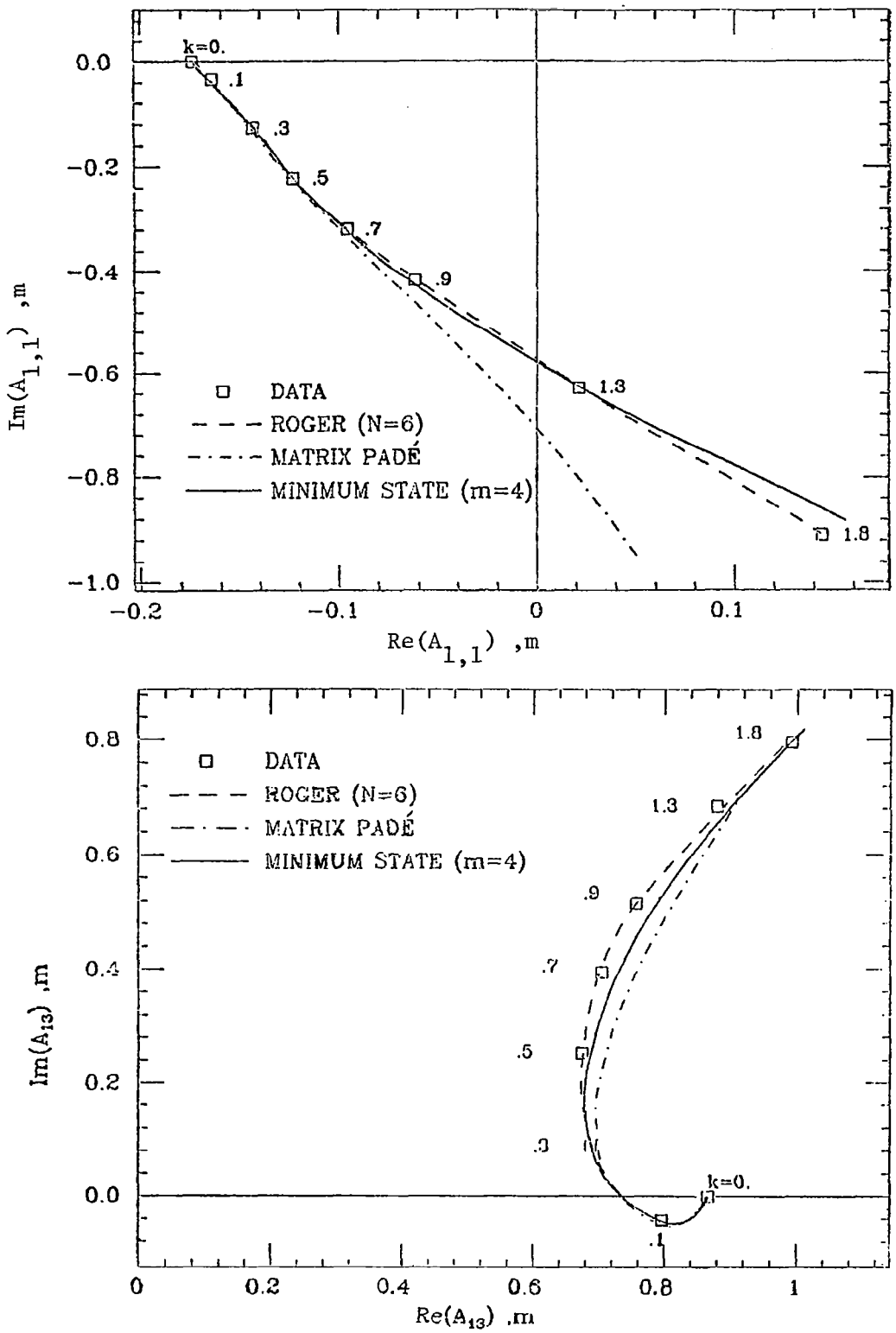

Figure 8: Rational approximations of aerodynamic coefficients, research wing at M=0.9.

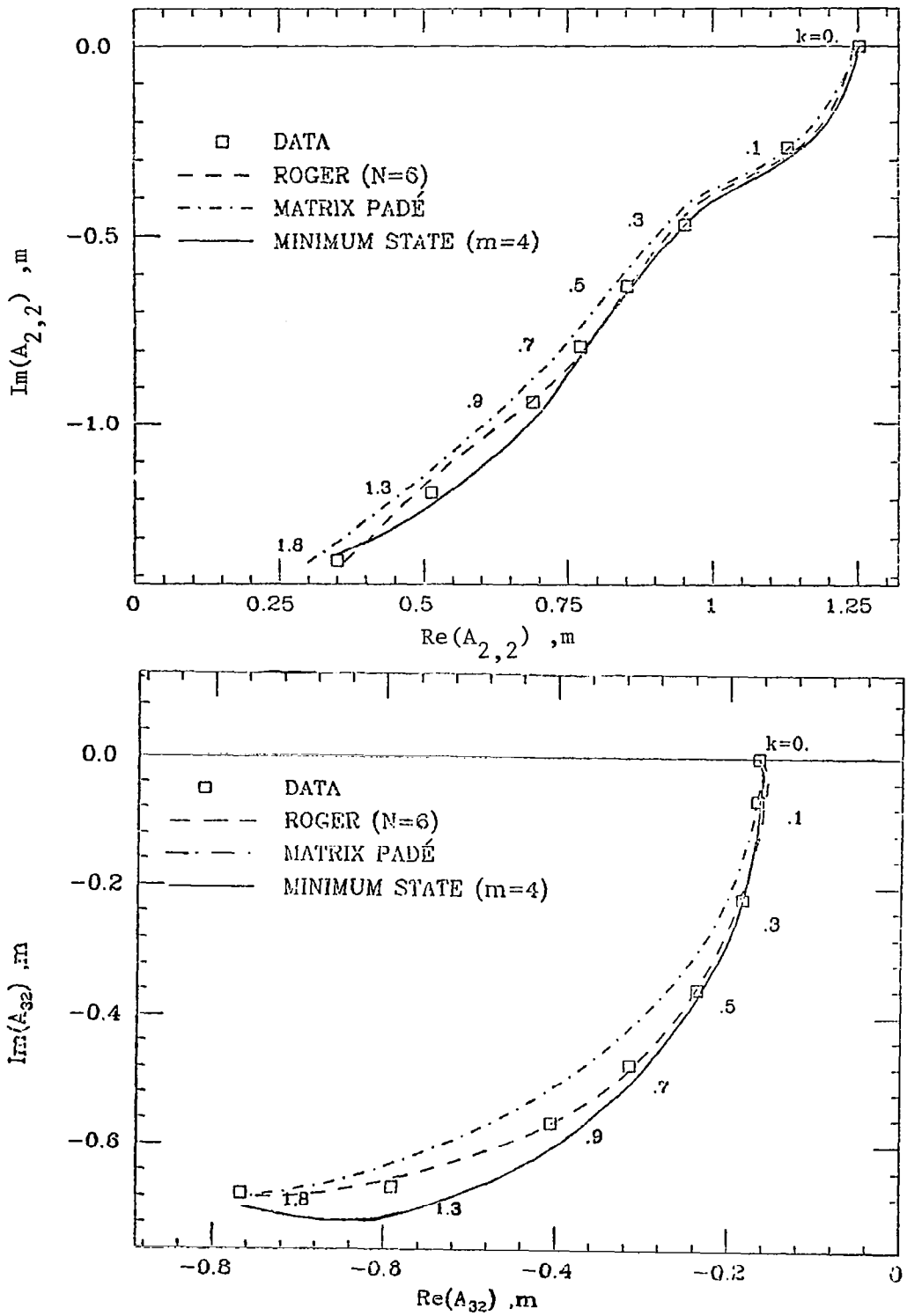

Figure 8 (Concluded)

ACTIVE FLUTTER SUPPRESSION AND GUST ALLEVIATION

Problem Definition and Design Strategy

The open-loop state-space aeroelastic equations of motion developed previously form the basis for control analysis. The purpose of this section is to demonstrate the use of some modern control techniques for flutter suppression and gust alleviation.

The structural properties and the variation of the aerodynamic influence coefficents over the flight envelope are assumed to be accurately known, and the aeroelastic system is assumed to be accurately represented by a finite-order state-space equation of motion. The system is subjected to random excitation by a vertical gust, which is defined in statistical terms by its mean-square velocity and power spectral density (PSD). The frequency dependent aerodynamic loads caused by the sinusoidal gust are known over the flight envelope.

The control means are aerodynamic control surfaces whose commanded rotations serve as input parameters. An arbitrary number of sensors measure discrete displacements, velocities or accelerations on the lifting surface. The measurements are assumed to be perfect. Compensator transfer functions close the loop by relating the control commands to the measurement signals. This is a constant parameter control system with no flight condition measurements.

A scalar design cost function is defined as a weighted sum of mean-square gust response parameters at selected points of the flight envelope. The compensator parameters are optimized to yield a minimal cost function. Careful choice of the cost function parameters leads to a control law, if there is any, which stabilizes the system throughout the entire flight envelope. The considerations in designing the cost function will be discussed subsequently.

Optimal control theory [34,45] supplies a straightforward optimal solution for a controllable and observable linear control system with fixed dynamics and quadratic cost function. The controller and observer dynamics are uncoupled (the separation theorem), and their separate solutions combine to a compensator of the order of the system. In our case, the dynamics vary over a wide range, and the separation theorem does not hold. Furthermore, a compensator of the order of the system is not of particular significance. The analysis is expected to yield a lower cost function as the compensator order is increased. On the other hand, increasing order means higher analysis, hardware and debugging costs and lower reliability. A practical approach is to design for the lowest order compensator which stabilizes the system over the entire flight envelope, meets the control system hardware limitations and yields satisfactory gust response.

The Control Equations

A block diagram of the closed-loop aeroelastic control system is given in Fig. 9. The open-loop equation of motion (4.23) is now

supplemented with a control input term. The formulation and later numerical examples are for a single-input control system. The extension to a multi-input system is straightforward, except for the pole assignment technique which is described later in this section. The plant equations with no process noise are

$$\underset{n_c x 1}{\{\dot{z}\}} = [F_1]\{z\} + \{G_1\}u \qquad , \qquad n_c = 2n+m \tag{5.1}$$

where $$\{z\} = \begin{Bmatrix} x \\ \dot{x} \\ x_a \end{Bmatrix} \quad , \quad \{G_1\} = \begin{Bmatrix} 0 \\ [M_s+M_a]^{-1}\{G_2\} \\ 0 \end{Bmatrix} \quad ,$$

$$[F_1] = \begin{bmatrix} 0 & [I] & 0 \\ -[M_s+M_a]^{-1}[K_s+K_a] & -[M_s+M_a]^{-1}[B_s+B_a] & [M_s+M_a]^{-1}[D] \\ 0 & [E] & [R] \end{bmatrix}$$

The state vector $\{z\}$ and the dynamic matrix $[F_1]$ were discussed previously. The control input u is the commanded value of the control surface rotation (β_c in Fig. 1). The actual control surface motion states are part of $\{z\}$. It is assumed that the actuator is a linear spring with no damping or delay, such that $\{G_2\}$ is a function of the actuator stiffness only. More complicated dynamics of the actuator system can be modeled by additional states or compensated for in the final control law [6]. While $[F_1]$ may vary considerably with Mach number M and dynamic pressure q the only term in $\{G_1\}$ which is a function of M and q is $[M_a]$, which is usually small with respect to $[M_s]$.

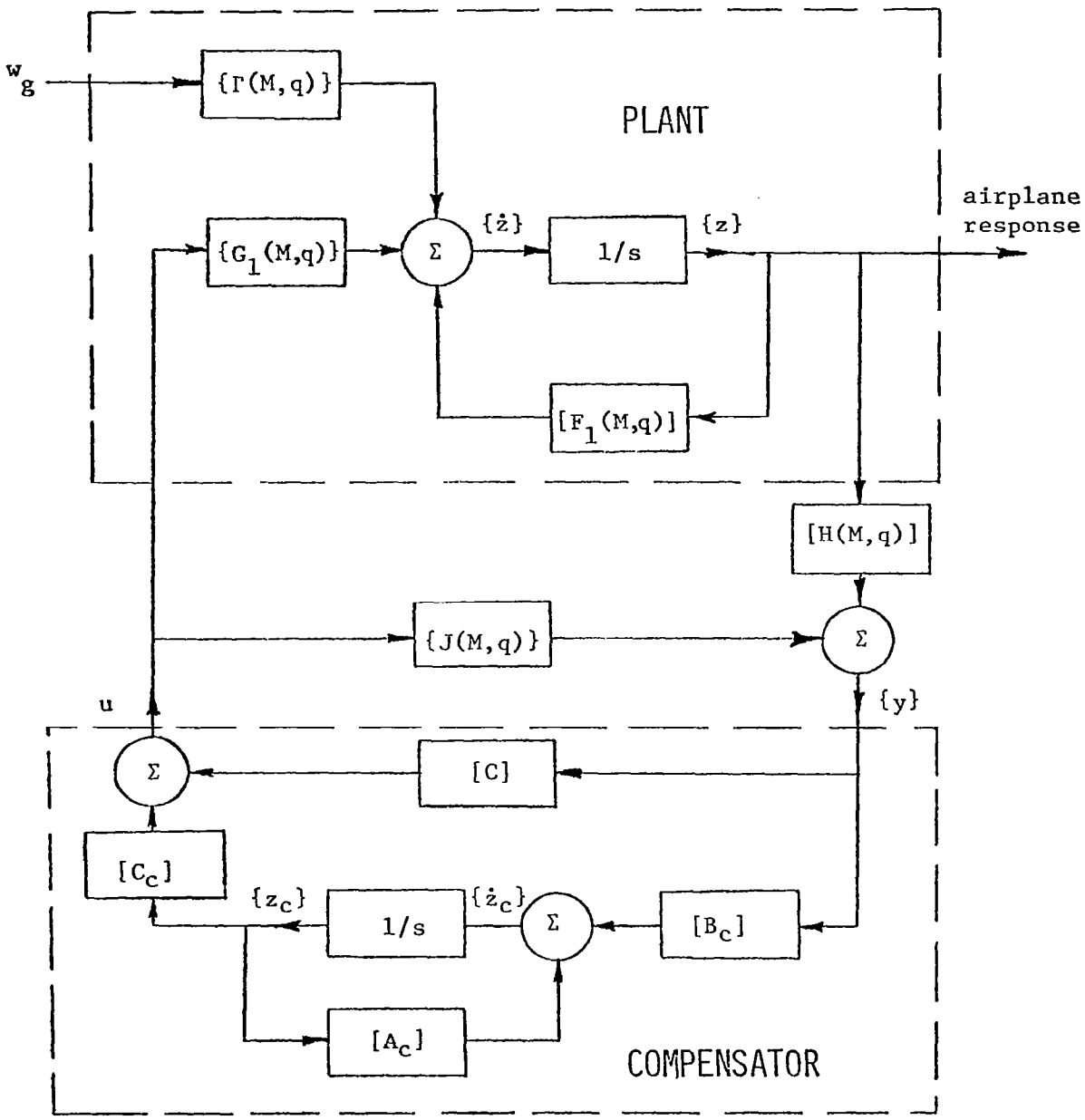

Figure 9: Block diagram of a closed-loop aeroelastic control system.

Sensors located at various points of the structure take measurements which combine to form the output (measurement) equation

$$\underset{m_c x 1}{\{y\}} = \underset{m_c x n_c}{[H]} \underset{n_c x 1}{\{z\}} + \{J\}u \qquad , m_c \leq n_c \tag{5.2}$$

where [H] can be partitioned as

$$[H] = \left[[H_d], [H_v], [H_a]\right]$$

The vector $\{y\}$ consists of discrete structural motion measurements, which are linear combinations of the modes which serve as structural generalized coordinates. When the measurements are displacement or velocity related, [H] is independent of M and q, $[H_a] = 0$ and $\{J\} = 0$. The most practical measurement devices, however, are accelerometers for which the measurement vector becomes

$$\{y\} = [H_0]\{\ddot{x}\} \tag{5.3}$$

where $[H_0]$ is defined by the modal displacements at the measurement points. Equation (5.1) is used to describe $\{y\}$ of Eq. (5.3) in the form of Eq. (5.2) with

$$[H] = [H_0][M_s+M_a]^{-1}\left[-[K_s+K_a], -[B_s+B_a], [D]\right] \tag{5.4}$$

and $$\{J\} = [H_0][M_s+M_a]^{-1}\{G_2\}$$

Now both [H] and $\{J\}$ are functions of M and q.

A compensator of the order of l_c adds l_c states to the system. Following the formulation of Ref. [35], the compensator states are described in a compensator canonical form as

$$\underset{l_c x 1}{\{\dot{z}_c\}} = [A_c]\{z_c\} + \underset{l_c x m_c}{[B_c]}\{y\} \tag{5.5}$$

where $$[A_c] = \begin{bmatrix} [A_{c1}] & 0 & \cdots & 0 \\ 0 & [A_{c2}] & & 0 \\ \vdots & & \ddots & \\ 0 & 0 & & [A_{ckc}] \end{bmatrix} \quad \text{with} \quad [A_{ci}] = \begin{bmatrix} 0 & 1 \\ a_{2i-1} & a_{2i} \end{bmatrix}$$

$$[A_{ckc}] = a_{1c} \text{ for odd } l_c$$

and $$k_c = \begin{cases} l_c/2 \text{ for even } l_c \\ (l_c+1)/2 \text{ for odd } l_c \end{cases}$$

Equations (5.1), (5.2) and (5.5) are combined to form the equations for the augmented system.

$$\begin{Bmatrix} \dot{z} \\ \dot{z}_c \end{Bmatrix} = \begin{bmatrix} [F_1] & 0 \\ [B_c][H] & [A_c] \end{bmatrix} \begin{Bmatrix} z \\ z_c \end{Bmatrix} + \begin{Bmatrix} \{G_1\} \\ [B_c]\{J\} \end{Bmatrix} u \tag{5.6}$$

When the loop is open (u=0), the plant and the compensator are obviously uncoupled. The loop is closed by a control law of the form

$$u = [C]\{y\} + [C_c]\{z_c\} \tag{5.7}$$

where $[C_c] = [[C_{c1}], [C_{c2}], \cdots, [C_{ckc}]]$

with $[C_{ci}] = [0 \quad 1]$ and $[C_{ckc}] = 1$ for odd l_c

An extension of $[C_c]$ to a multi-input system is given in Ref. [34]. Substituting Eq. (5.2) into Eq. (5.7) gives

$$u = [C'][H]\{z\} + [C_c']\{z_c\}, \tag{5.8}$$

where $[C'] = \dfrac{1}{1-[C]\{J\}}[C]$ and $[C_c'] = \dfrac{1}{1-[C]\{J\}}[C_c]$

Substituting Eq. (5.8) into Eq. (5.6) gives

$$\begin{Bmatrix} \dot{z} \\ \dot{z}_c \end{Bmatrix} = \begin{bmatrix} [F_1]+\{G_1\}[C'][H] & \{G_1\}[C_c'] \\ [B_c]+[B_c]\{J\}[C'][H] & [A_c]+[B_c]\{J\}[C_c'] \end{bmatrix} \begin{Bmatrix} z \\ z_c \end{Bmatrix} \tag{5.9}$$

This is the closed-loop system equation of motion with no process noise. For no flutter in the flight envelope, all the eigenvalues of Eq. (5.9) should have negative real parts over the entire range of M and q. For a given system with m_c measurements, the free design parameters are the m_c gains in $[C]$, compensator order l_c, dynamics parameters a_1 through a_{lc} and the $l_c x m_c$ parameters in $[B_c]$.

The cost function and the parameter optimization are discussed next, followed by discussion of the cases of zero-order and second-order compensators.

Cost Function and the Optimization Procedure

The cost function for which the free control parameters are optimized is based on the airplane response to atmospheric turbulence, which was

discussed earlier. In modern control terminology, the vertical component of the turbulence-induced gust velocity can be described as a process noise, as shown in the block diagram of Fig. 9. The plant Eq. (5.1) becomes

$$\{\dot{z}\} = [F_1]\{z\} + \{G_1\}u + \{\Gamma\}w_g \tag{5.10}$$

where $$\{\Gamma\} = \begin{Bmatrix} 0 \\ q/V[M_s+M_a]^{-1}\{A_g(ik)\} \\ 0 \end{Bmatrix}$$

As discussed previously, W_g is defined in statistical terms by its mean-square σ_{wg}^2, its power spectral density (PSD) Φ_{wg}, and zero mean value. As shown in Fig. 3, the PSD is far from that of white noise. The distribution matrix $\{\Gamma\}$, in addition to being a function of M and q, is a function of the frequency ω. The closed-loop gust response is calculated by the continuous gust response equations, modified to include the rational approximation of the aerodynamic influence coefficients and the control terms.

The process noise term of Eq. (5.10) can be added to Eq. (5.9), which can be then solved for the gust frequency response of the whole system. Advantage is taken, however, of the special characteristics of the system, such that a much lower-order system of equations is solved. Since the measurements are of structural motion only, vector $\{y\}$ of Eq. (5.2) can be defined as

$$\{y\} = [H_d]\{x\} + [H_v]\{\dot{x}\} + [H_b]\{\ddot{x}\} \tag{5.11}$$

To relate the frequency response of u to that of $\{x\}$, the variables of Eqs. (5.5), (5.7) and (5.11) are replaced by their frequency response, which yields

$$U(i\omega) = [C_2]\{X(i\omega)\} \tag{5.12}$$

where $$[C_2] = \left([C]+[C_c]\left[i\omega[I]-[A_c]\right]^{-1}[B_c]\right)\left([H_d]+i\omega[H_v]-\omega^2[H_0]\right)$$

From the second partition of Eq. (5.10), with the matrix definitions of Eq. (5.1), we obtain the equivalent of Eq. (3.9) for the closed-loop gust frequency response of the structural degrees of freedom. This equation is

$$\left[-\omega^2[M_s+M_a]+[K_s+K_a]+i\omega[B_s+B_a]-i\omega[D]\left[i\omega[I]-[R]\right]^{-1}[E]\right.$$

$$\left.-\{G_2\}[C_2]\right]\{X(i\omega)\} = (q/V)\{A_g(ik)\} \tag{5.13}$$

Equation (5.13) consists of n equations to be simultaneously solved for $\{X(i\omega)\}$. Calculating the frequency response from Eq. (5.10) would require solving $2n+m+m_c$ equations simultaneously. The design frequency response of Eq. (3.10) is now modified to include a control term,

$$Z_d(i\omega) = \left([a_d]+i\omega[a_v]-\omega^2[a_0]\right)\{X(i\omega)\} + a_u U(i\omega) \tag{5.14}$$

where $U(i\omega)$ is calculated from $\{X(i\omega)\}$ using Eq. (5.12).

The design mean-square frequency response σ_{zd}^2 is calculated by Eq. (3.16). Referring σ_{zd}^2 and $Z_d(i\omega)$ to a point i in the flight envelope, defined by M and q, Eq. (3.16) becomes

$$\sigma_{zd,i}^2 = \int_0^\infty |Z_{d,i}(i\omega)|^2 \Phi_{wg}(\omega) d\omega \qquad (5.15)$$

The integration is done numerically, using the trapezoid rule [48], from zero to a frequency 50% higher than the highest imaginary part of the eigenvalues of Eq. (5.9).

The mean-square response of Eq. (5.15) serves as a local cost function. A global cost function is defined as weighted sum of local cost functions at selected points of the flight envelope

$$J_0 = \sum_i a_{g,i} \sigma_{zd,i}^2 \qquad (5.16)$$

The free control parameters, which were discussed in Section 5.2, are optimized for a minimal global cost function J_o by using Davidon's minimization method [37], as modified by Stewart [39] to accept different approximations of derivatives.

The number of flight envelope points participating in J_o is limited by computer cost, as a gust response function evaluation is required in each step of the numerical integration of Eq. (5.15). The flight envelope points should include:

1. Normal operation points (see Fig. 2) to minimize turbulence-induced vibrations and control activity during cruising flight.

2. Points within the safety margin envelope at which structural or control hardware limitations are exceeded.

3. Points which might become unstable during the optimization process.

It is clear that the points of the second and third categories above may not be anticipated in advance. After an optimization is performed for some cost function, root loci and critical response parameters are calculated for more points in the flight envelope. If the results are not satisfactory, the cost function is modified, and the optimization is repeated, starting with the previous optimized control parameters.

Gust response is infinitely large for points with pure imaginary roots. At each optimization cycle the initial control parameters should stabilize the system at all the cost function points. If the control means are sufficient, the optimization procedure tends to move roots of cost-function points, which are very close to the s-plane imaginary axis, away to the left. Thus, whenever a root-loci branch crosses to the right-hand plane within the flight envelope, a point close to the crossing point (but still stable) is added to the cost function. The weights $a_{g,i}$ assigned to the stability-related points, are relatively small to avoid unnecessary performance deterioration at normal operation points.

When the control system is unable to provide satisfactory results, the design can be repeated with a higher order compensator. If the improvement is not significant, a change in the number of sensors or their

locations, or in the size and location of the control surfaces, is needed. Sensor and control surface design, however, is beyond the scope of this study.

Pole Assignment

When a single-input, multi-output aeroelastic system is controlled by a direct, partial-feedback control law (zero-order compensator), the only free parameters are the gains [C] of Eq. (5.7). The optimization procedure can now be applied to find the "best" control gains. Better insight and more efficient use of the optimization routine may be achieved, however, when assigned poles replace the control gains as free parameters in the optimization.

The Laplace transform of Eqs. (5.1) and (5.2) yields the input-output transfer function

$$\frac{\{Y(s)\}}{U(s)} = [H]\left[s[I]-[F_1]\right]^{-1}\{G_1\} + \{J\} \tag{5.17}$$

Substituting Eq. (5.7) with $[C_c] = 0$ into Eq. (5.17) and premultiplying both sides by [C] gives

$$[C]\left([H]\left[s[I]-[F_1]\right]^{-1}\{G_1\}+\{J\}\right) = 1 \tag{5.18}$$

or

$$[C]\left([H]\{g(s)\}+D_0(s)\{J\}\right) = D_0(s) \tag{5.19}$$

where

$$\{g(s)\} = \left(\text{adj}\left[s[I]-[F_1]\right]\right)\{G_1\} \quad , \quad D_0(s) = \left|s[I]-[F_1]\right|$$

In polynomial form

$$\{g(s)\} = \left[\sum_{i=0}^{n_c} [N_i] s^{nc-i}\right]\{G_1\} \tag{5.20}$$

and

$$D_0(s) = \sum_{i=0}^{n_c} Q_i s^{nc-i} \tag{5.21}$$

An efficient algorithm for calculating the polynomial coefficients of $\{g(s)\}$ and $D_o(s)$ is given by Kailath [49]. The algorithm reads

$$\begin{aligned} [N_1] &= [I] \\ Q_i &= -(1/i)\,\text{trace}([N_i][F_1]) \qquad \text{for } i = 1, n_c \\ [N_i] &= [N_{i-1}][F_1] + Q_{i-1}[I] \qquad \text{for } i = 2, n_c \end{aligned} \tag{5.22}$$

Once the polynomial coefficients are calculated for a point in the flight envelope, one equation (5.19) is constructed for each assigned closed-loop pole at this point. A complex pole assignment gives two equations, one for the real and one for the imaginary part of Eq. (5.19). A set of m_c assigned poles gives m_c equations to be solved for [C]. Different poles can be assigned for different flight conditions.

Once the control gains are found, the closed-loop poles at any flight condition can be found by solving the eigenvalue problem

$$\left[[F_1] + \frac{1}{1-[C]\{J\}}\{G_1\}[C][H]\right]\{Z(s)\} = s\{Z(s)\} \tag{5.23}$$

Typical Section with Zero-Order Compensator

A zero-order compensator is designed for the typical section of Fig.1 in incompressible flow. The structural and aerodynamic data sources are summarized in Table 2. The minimum-state approximated aerodynamic coefficients, described in the first minimum state numerical example are used to model the system with six structural states and two augmented states.

The variables of Eq. (5.1) are $\{z\}^t = [h,\alpha,\beta,\dot{h},\dot{\alpha},\dot{\beta},x_{a1},x_{a2}]$ and $u = \beta_c$. The independent variable of the root loci, which defines the flow conditions, is the non-dimensionalized velocity $V/b\omega_\alpha$. The open-loop ($\beta_c = 0$) root loci (Fig. 10) show a violent plunge-torsion flutter at $V/b\omega_\alpha = 3.02$. The control system is required to ensure no flutter between $v/b\omega_\alpha = 1.$ and 3.5, and to minimize the cost function of Eq. (5.16) as defined in Table 6 for five different design cases. In all cases, the process noise is vertical gust velocity w_g, defined by Dryden's PSD of Eq. (3.13) with $\sigma_{wg}^2 = 1.0\ b^2/sec^2$ and $L_g = 50\ b$. The gust forcing vector, $\{A_g\}$ of Eq. (5.13), is derived in Appendix A following Bisplinghoff et al. [10].

The closed-loop root loci of cases 3 and 4 of Table 6 are given in Fig. 11. The mean-square response of $\dot{\beta}$ for all the cases is given in Fig. 12. The mean-square responses of $\dot{h}$ and $\dot{\alpha}$ for cases 3, 4 and 5 are compared to the open-loop response in Fig. 13.

Assigned complex poles at $V/b\omega_\alpha = 3.5$ were used as optimization driving parameters, one complex pair in the two-measurement cases and two pairs in the four-measurement cases. Early analysis, with only one cost

TABLE 6

Typical section control design cases

Case	Measurements	Design response parameter, z_d	Cost function	
			points, $V/b\omega_\alpha$	weights, $a_{g,i}$
1	$\dot{h},h$	β	2.5, 3.2	1., 1.
2	$\dot{h},h,\dot{\alpha},\alpha$	β	2.5, 3.2	1., 1.
3	$\dot{h},h$	β	2.5, 2.85, 3.2	1., 4., 1.
4	$\dot{h},h,\dot{\alpha},\alpha$	β	2.5, 2.85, 3.2	1., 4., 1.
5	$\dot{h},h$	$\dot{h}+3\alpha$	2.5, 2.85, 3.2	1., 4., 1.

function point at $V/b\omega_\alpha = 2.5$, resulted in instability between $V/b\omega_\alpha = 3.25$ and 3.4. This problem was solved by adding $V/b\omega_\alpha = 3.2$ to the cost function points (cases 1 and 2). As shown in the upper part of Fig. 12, the mean-square response of the design parameter β at the cost function points is reduced by increasing the number of measurements (as expected). In between the design points, however, there are response peaks, with the four-measurement case being more sensitive to changes in flow conditions.

Adding the response at $V/b\omega_\alpha = 2.85$ to the cost function (cases 3 and 4) moves the peaks and the sensitive region to higher velocities (lower part of Fig. 12). The root loci of cases 3 and 4 (Fig. 11) show

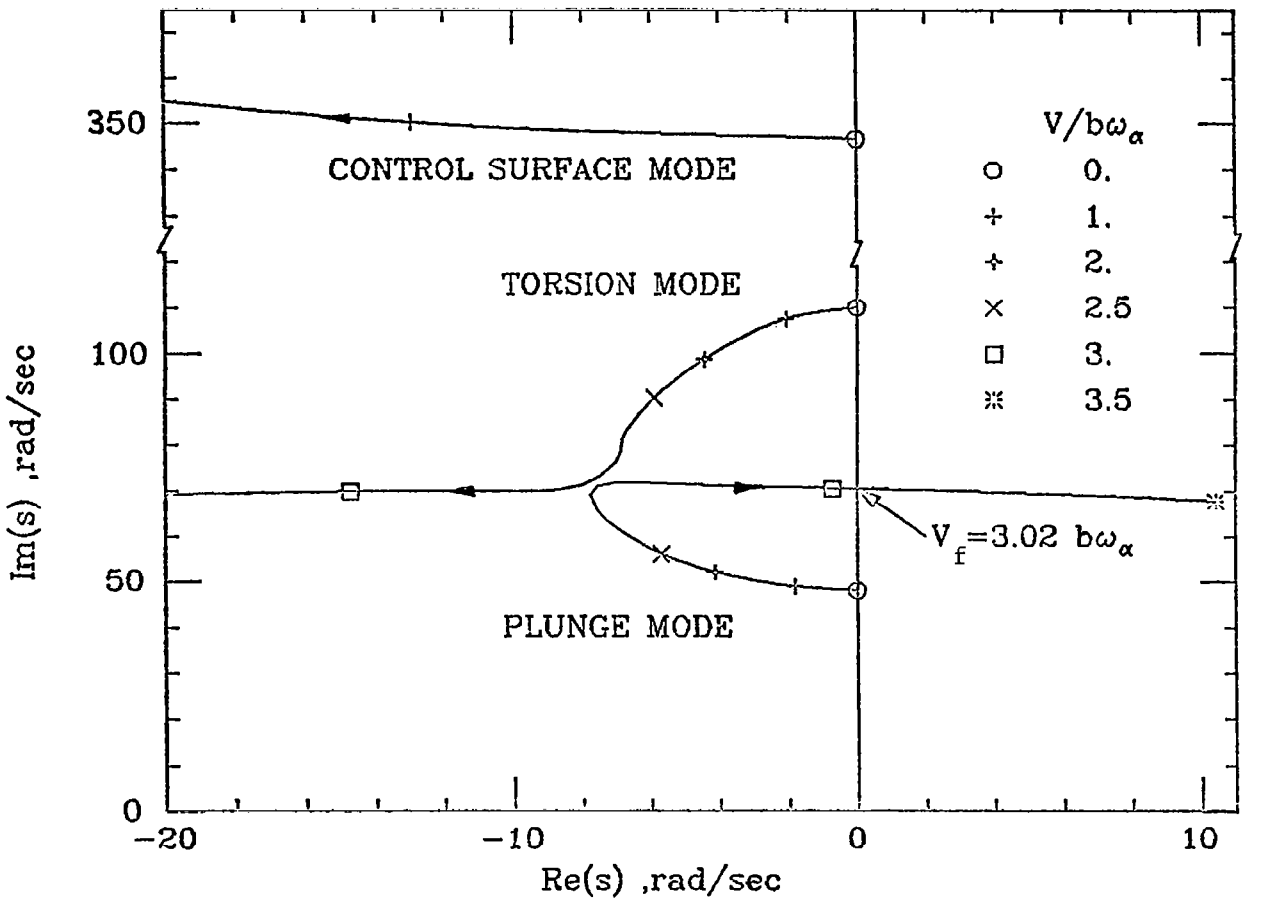

Figure 10: Open-loop root loci of a typical section in incompressible flow.

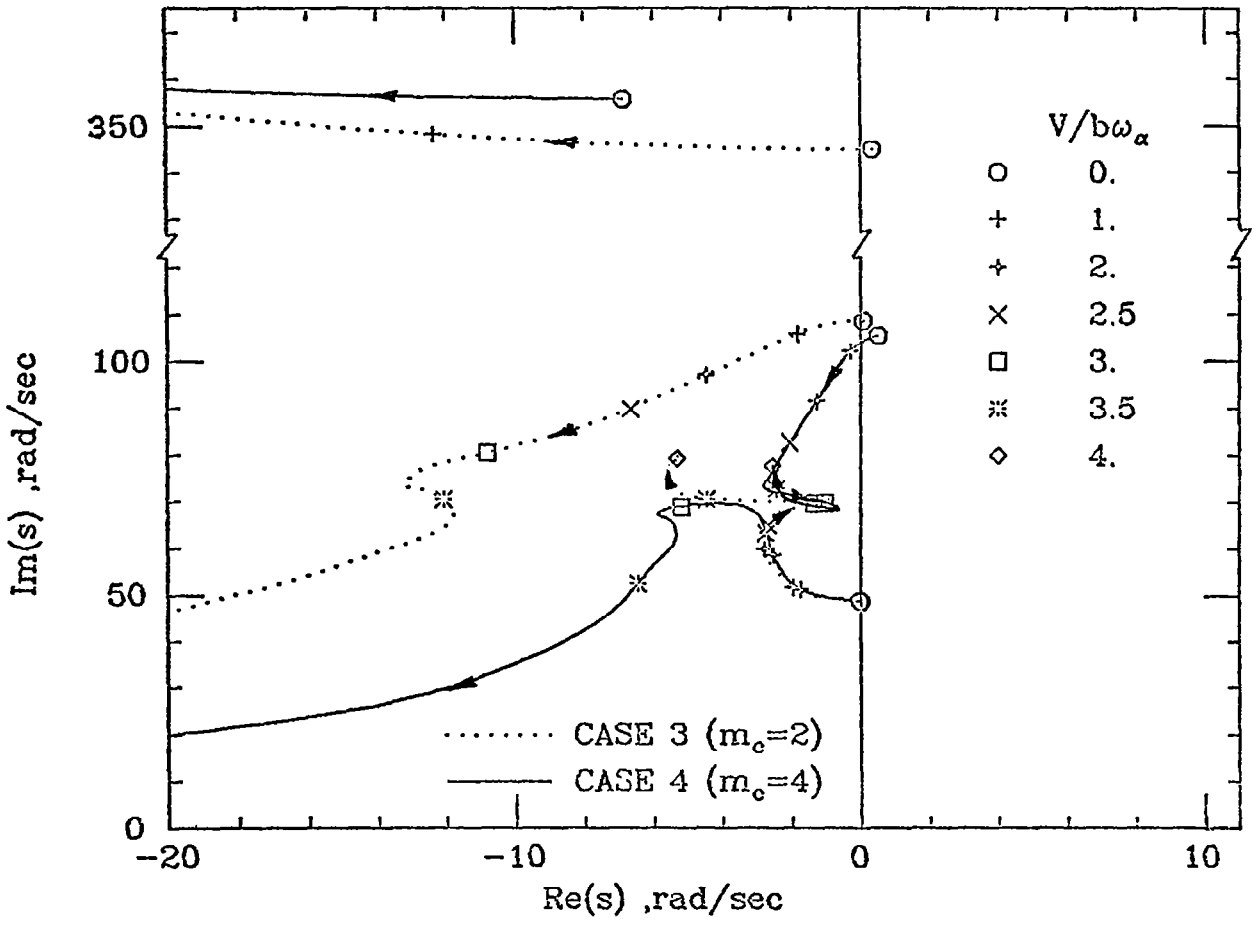

Figure 11: Closed-loop root loci of a typical section in incompressible flow.

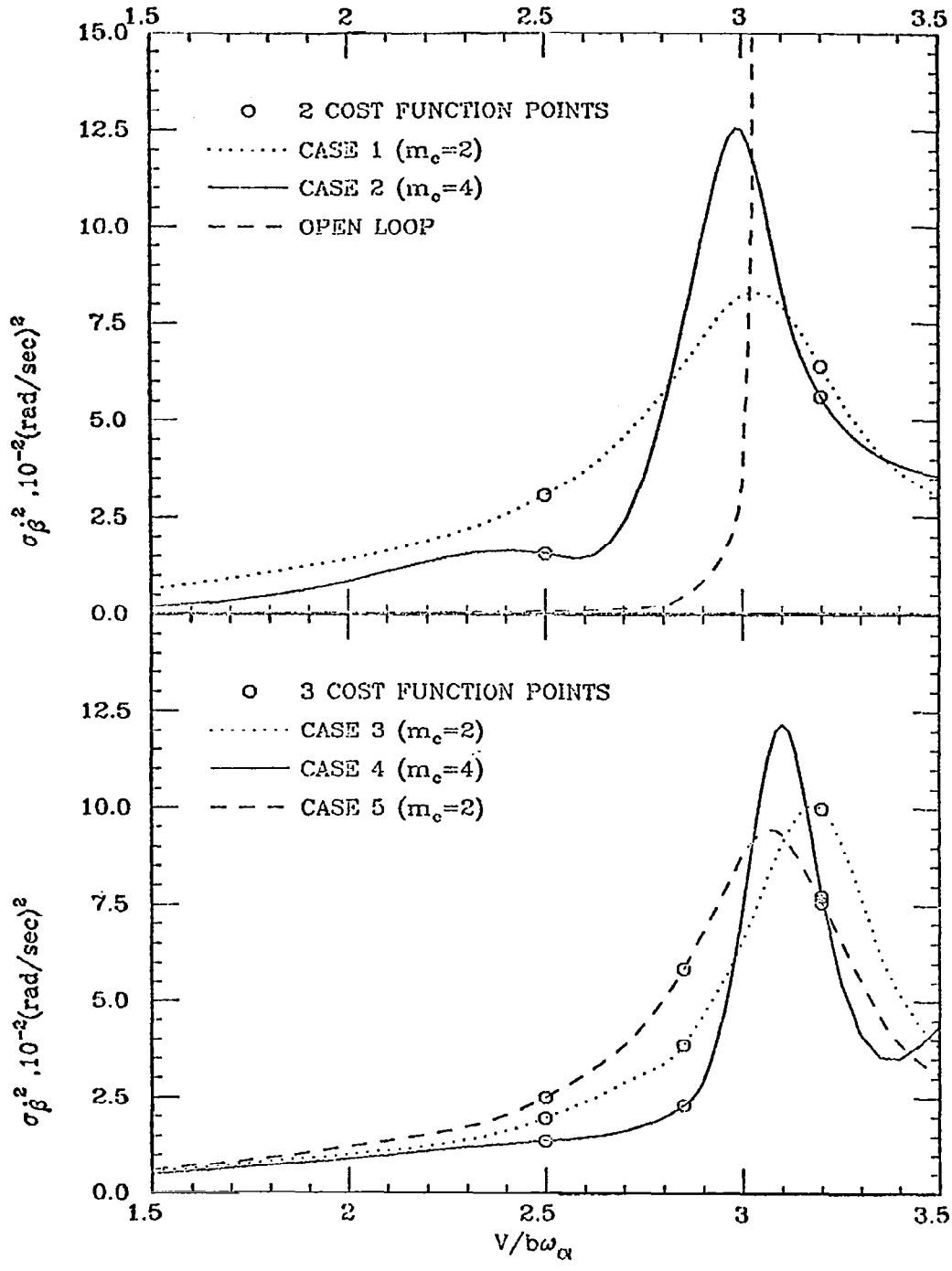

Figure 12: Control surface turbulence response, typical section in incompressible flow.

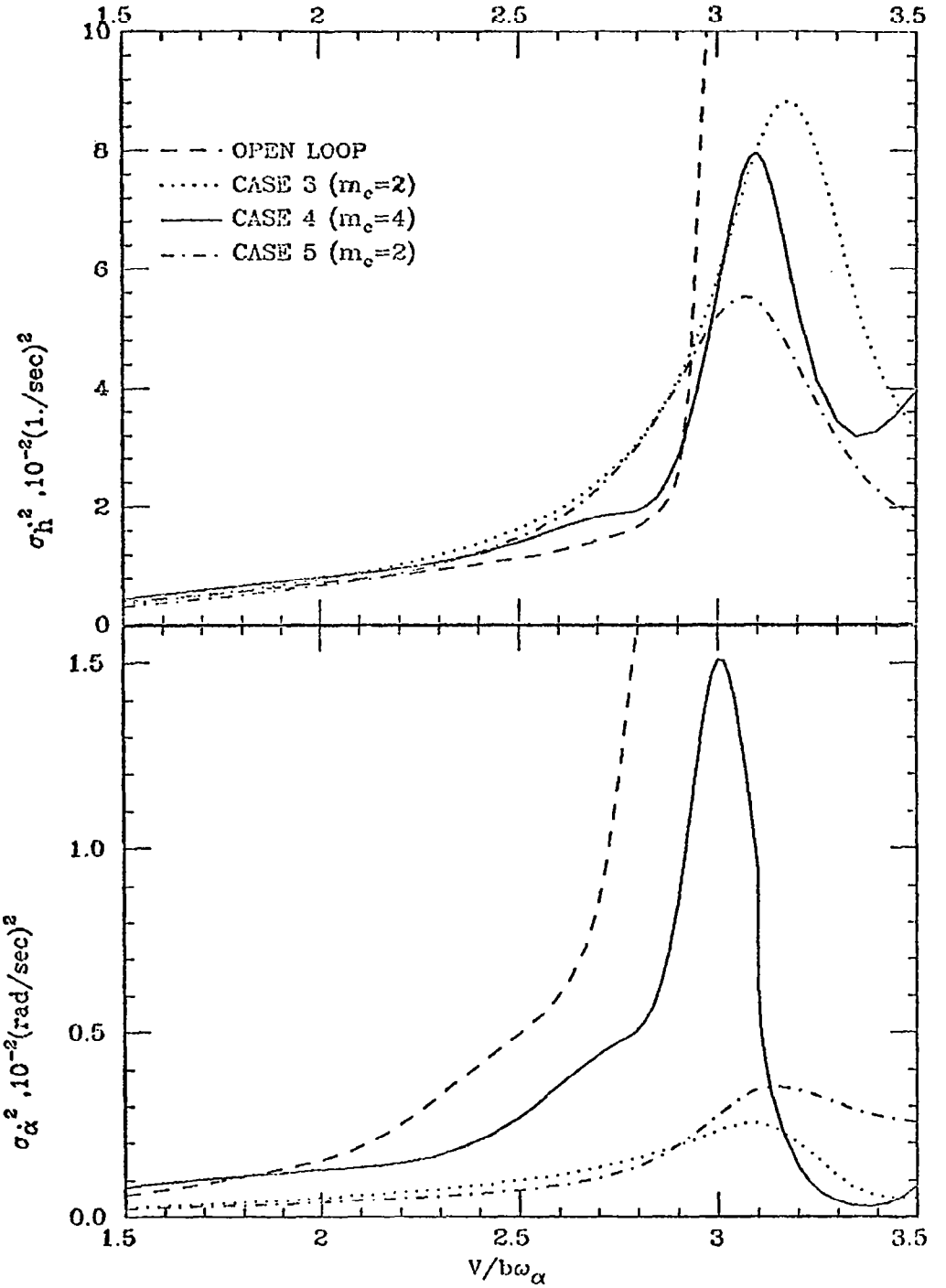

Figure 13: Plunge velocity and pitch rate turbulence response, typical section in incompressible flow.

that the two modes which participate in the open-loop flutter mechanism (Fig. 10) still interact with each other. But instead of the violent flutter, a more complicated interaction, which keeps the system stable, is observed. The only instabilities occur at very low velocities as a result of the wing-control-surface inertial coupling. This problem is easily solved by switching the control system on only after takeoff.

Figure 13 shows for cases 3 and 4 the mean-square gust responses for the translation and pitching velocities, when they are not included in the cost function. The closed-loop plunge velocity responses $\sigma_{\dot{h}}^2$ are higher than the open-loop response at subflutter velocities and have sharp peaks at higher velocities. The closed-loop pitch rate responses $\sigma_{\dot{\alpha}}^2$ are generally lower than the open-loop responses, with the two-measurement case giving much lower responses than the four-measurement case. The main point is that one should keep careful track of response parameters which are not included in the cost function.

A change in the design parameter of the two-measurement case to $z_d = \dot{h} + 3\dot{\alpha}$ (case 5) lowers the plunge velocity response $\sigma_{\dot{h}}^2$ at the high airspeed range without changing the subflutter response significantly. The improvement in $\sigma_{\dot{h}}^2$ is accompanied (as expected) by deteriorating overall $\sigma_{\dot{\beta}}^2$ (Fig. 12).

Research Wing with Zero and Second-Order Compensators

A compensator is designed to increase the flutter dynamic pressure of the research wing of Fig. 4, using a single accelerometer signal and minimal control surface mean-square rotation rate.

The structural and aerodynamic data sources are summarized in Table 2. The structural modal properties, as defined in Eq. (2.15), are given in Table 7. The control surface is assumed to be structurally uncoupled from the wing. Its natural frequency was arbitrarily chosen to be well above the highest wing frequency in this analysis, and the mode shape consists of one radian control surface rotation. Open-loop calculations by Abel [6] indicate that higher vibration modes do not affect the lowest speed flutter mechanism.

TABLE 7

Structural modal properties of the research wing

Mode	Natural frequency, $\omega_{n,i}$ (rad/sec)	Generalized mass, $M_{s,ii}$	Modal Damping, ζ_i	Modal deflection at sensor location, Ψ_i (see Fig. 4)
first bending	32.88	1. kg	.005	0.4812
torsion	120.19	1. kg	.005	-0.2282
second bending	161.91	1. kg	.005	0.2002
control surface rotation	400.0	.0004 kg-m^2	.005	0.0

The flight envelope for this design consists of one Mach number, M = 0.9, and constant air velocity, V = 450 ft/sec (137.16 m/sec), such that

the independent variable is the dynamic pressure q. This representation fits a wind tunnel test [6]. For a given Mach number in atmospheric flight, the flight velocity varies somewhat with q because of the change in the speed of sound with altitude.

The fourth-order minimum-state approximation of the aerodynamic influence coefficients described in the last minimum state numerical example is used to construct the plant equation (5.1). The gust coefficients $\{A_g(ik)\}$ of Eq. (5.13) are interpolated by Roger's approximation (Eq. (4.5)) with N=6 and γ_i values of 0.2, 0.4, 0.6 and 0.8. Von Karman's power spectral density (Eq. (3.14)) represents the vertical gust velocity, with $\sigma_{wg}^2 = 1.0\ m^2/sec^2$ and $L_g = 100$ ft (30.48 m). The measurement equation (5.2) parameters are defined by Eq. (5.4), where the row vector $[H_0]$ takes the Ψ_i values of Table 7.

The open-loop root loci of the wing modes (Fig. 14) show an open-loop first-bending-torsion flutter at dynamic pressure $q_f = 5.37$ kPa. Previous control designs for this model [6,32] resulted in closed-loop flutter dynamic pressures between 9.3 and 9.8 kPa, with compensators of the order of 4 or more. The design target here is to achieve similar results with a lower order compensator, optimized for minimal cost function $J_0 = \sigma_\beta^2$ at q = 7 kPa.

The first trial involved the use of a zero-order compensator. Since the system is single-input single-output, the only free parameter is a single gain C of Eq. (5.7). Closed-loop calculations for various C values indicate very limited performance. Two typical closed-loop root loci are shown in Fig. 14. A positive control gain reduces both first

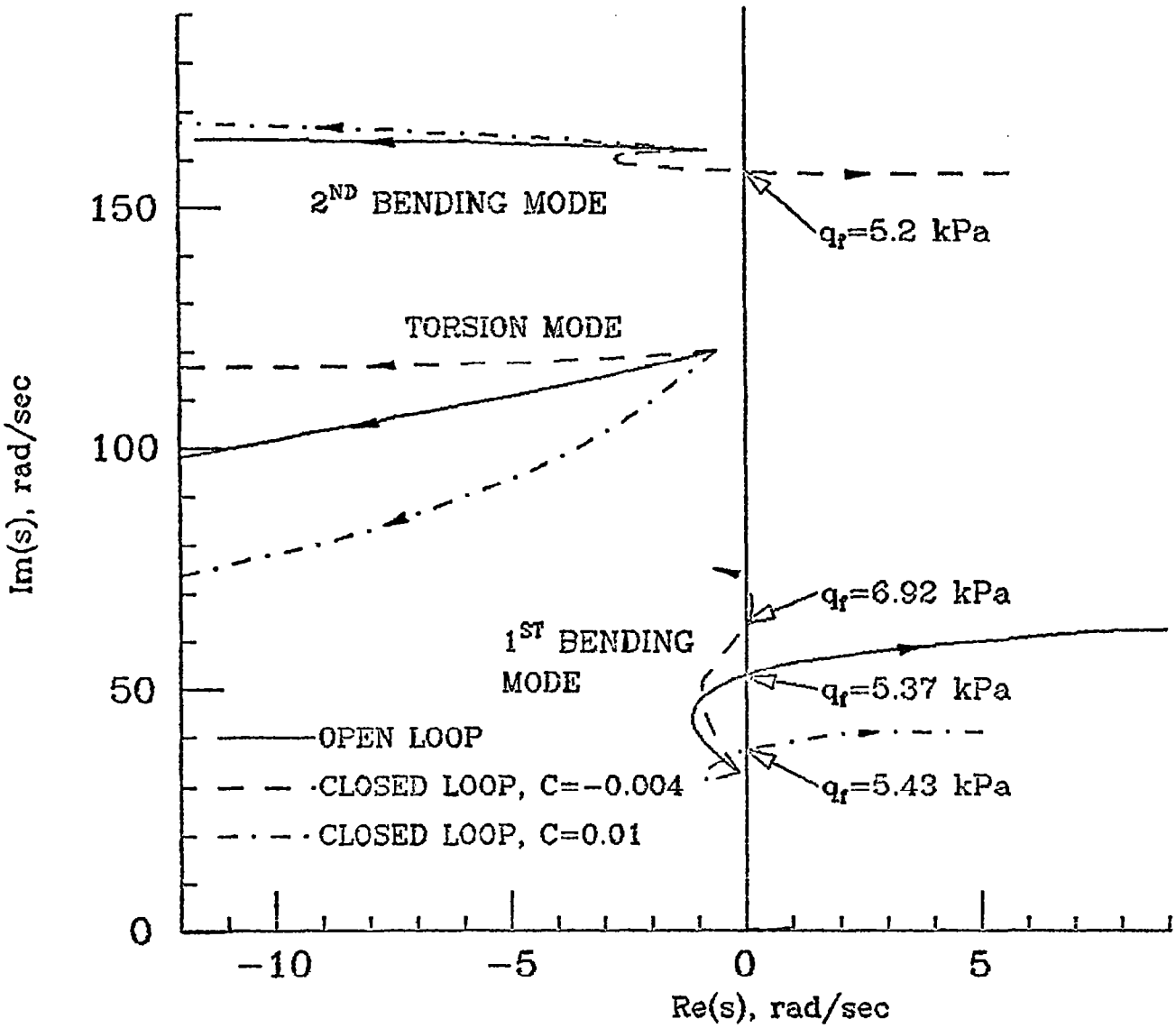

Figure 14: Open- and closed-loop root loci of the research wing modes with a zero-order compensator at M=0.9

bending and torsion frequencies with a very small effect on the flutter dynamic pressure. A negative control gain decouples the modes of the open-loop flutter mechanism but causes torsion-second-bending flutter. The variation of flutter dynamic pressure with control gain is shown in Fig. 15. Only 10% increase in flutter dynamic pressure is achieved in the very gain-sensitive region of the intersection of the two flutter mechanisms, thus this compensator is of little value.

In the second-order compensator design, the direct control gain is set to C = 0. Since $l_c = 2$ and $m_c = 1$, the only free compensator parameters are a_1, a_2 and $[B_c]$ (1x2) of Eq. (5.5). The optimal parameters are $a_1 = -351.14$, $a_2 = -28.51$ and $[B_c]^t = [-0.1819, -0.07653]$. The open- and closed-loop root loci of the wing modes are shown in Fig. 16. The control system has a considerable effect on the aeroelastic behavior, and the flutter dynamic pressure is increased to 9.93 kPa. The compensator mode interacts with the first bending mode, which gains substantial damping before fluttering. The torsion and second bending modes start to develop a flutter mechanism, as indicated by the turn of the second bending mode root locus, but they produce no flutter up to 10 kPa.

The variation of σ_β^2 and σ_β^{*2} of the closed-loop system with dynamic pressure is shown in Fig. 17. The response increases monotonically with dynamic pressure, and it does not show the sensitivity of the typical section discussed as the preceding example.

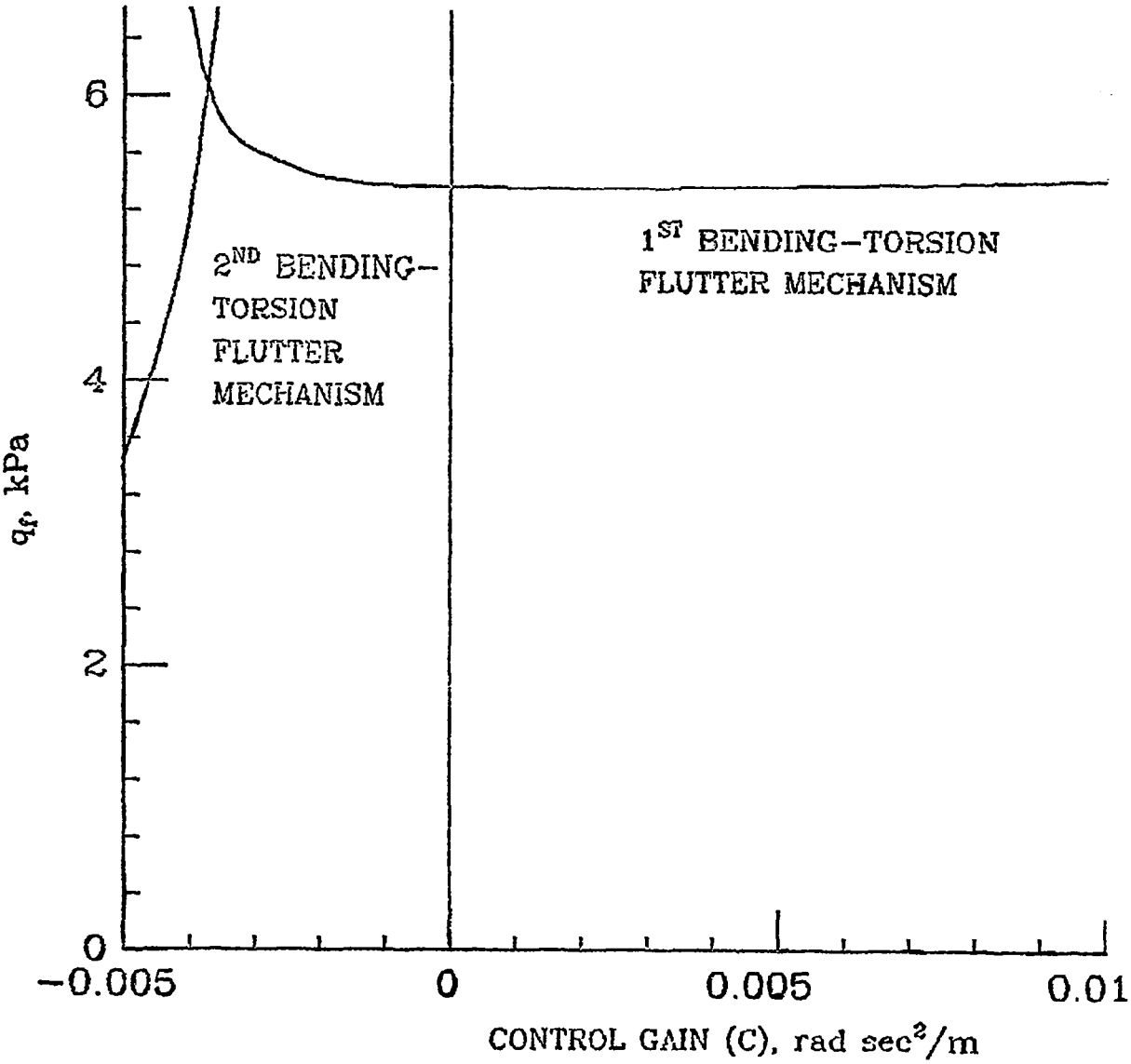

Figure 15: Variations of the research wing flutter dynamic pressure with a zero-order compensator control gain

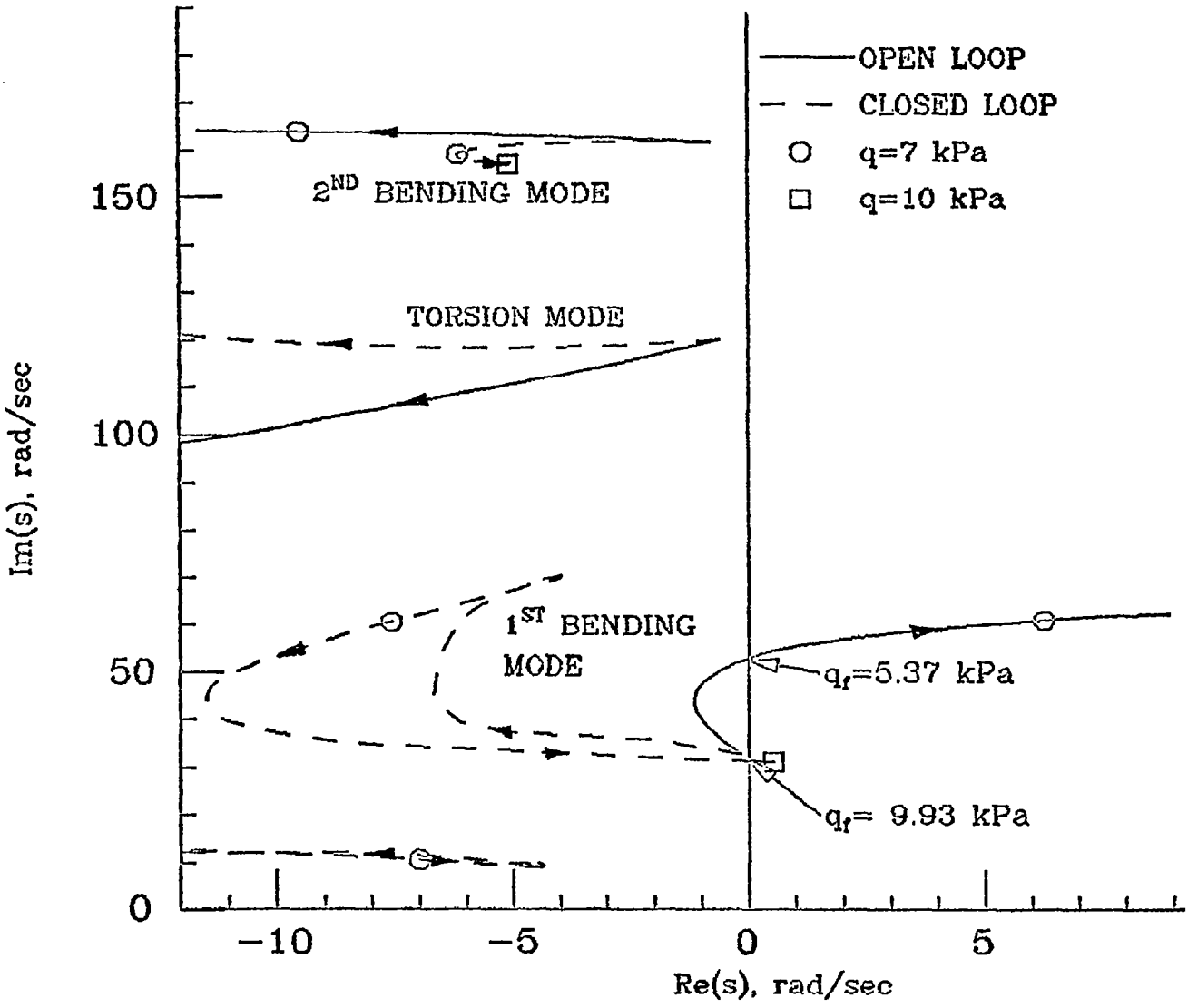

Figure 16: Open- and closed-loop root loci of the research wing modes with a second-order compensator at M=0.9

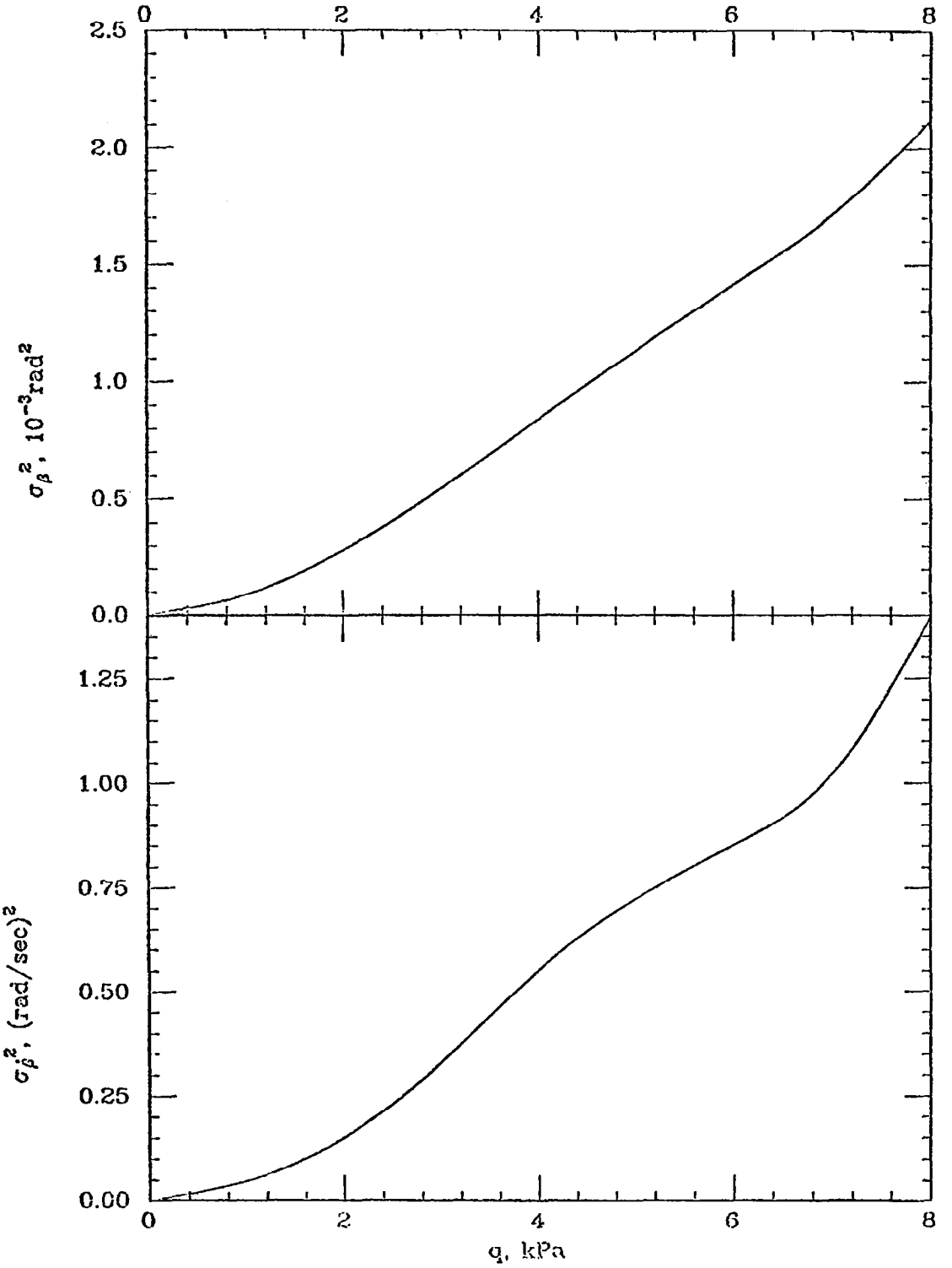

Figure 17: Closed-loop control surface turbulence response, research wing at M=0.9

PASSIVE FLUTTER SUPPRESSION

While active flutter suppression systems are still in the theoretical and experimental stages, passive flutter suppression means (namely structural modification techniques) are well established and widely used in the aerospace industry. Optimization procedures to meet flutter requirements with minimal weight penalty are given by Markowitz and Isakson [40] and by Haftka and Starnes [41]. These procedures are based on repetitive flutter analysis for varying structural parameters.

An active control system is a method for providing satisfactory flutter characteristics with no major structural changes, and thus with only a small weight penalty. The designer, however, should not overlook local structural modifications as flutter suppression means. Well placed concentrated masses or properly tuned springs can suppress flutter, as demonstrated in Ref. [42] for wing-store configurations. Local passive control means are formulated in the following discussion as subcases of active control means, such that a unified active-passive analysis can be performed using the methods of the preceding section.

Adding a Concentrated Mass

Although termed as "passive," a concentrated mass m_p, added to a given structure, is actually a perfect zero-order compensator. It measures acceleration and responds with a proportional force.

The basic assumption of modal analysis is that the motion of the structure, before and after the structural changes, is a linear combination of the modes which serve as generalized coordinates. This assumption is never exact for a continuous structure represented by a finite number of modes. The analyst should evaluate the assumption's accuracy by engineering judgment or by repeating the analysis with a higher number of modes.

In terms of the control terminology used in this paper, the measurement is the acceleration at the point where the concentrated mass is added. Equation (5.3) becomes

$$y = [H_0]\{\ddot{x}\} \qquad \text{where} \qquad [H_0] = \{\Psi_p\}^t \tag{6.1}$$

and where $\{\Psi_p\}^t$ is the modal deflection row vector at this point. The measurement equation (5.2) is constructed using Eq. (5.4). The control variable is the reaction force applied by the mass. Equation (5.7) becomes

$$u = Cy \qquad \text{where} \qquad C = -m_p \tag{6.2}$$

The plant equations (5.1) are constructed by leaving the system open-loop dynamic matrix $[F_1]$ untouched and using

$$\{G_2\} = \{\Psi_p\} \tag{6.3}$$

With the additional mass defined as input and output terms of the control equations, it can be superimposed on the active control equations. The cost function may be supplemented with a weighted mass penalty term, and the control gain (added mass) can be determined by the cost function minimization routine. The additional mass is limited, of course, to positive values unless a parasite mass already exists at this point.

The typical section in incompressible flow (see Fig. 1 and Table 2) was used to illustrate the effect of adding a concentrated mass. The changes in flutter velocity with additional mass at distance δb rearwards of the elastic axis (E.A.) are shown in Fig. 18. Since the elastic axis is located at $a = -0.4$, the leading edge is at $\delta = -0.6$ and a reasonable most forward mass location is around $\delta = -0.5$. The flutter velocity can be increased by approximately 20% with 20% total mass increase.

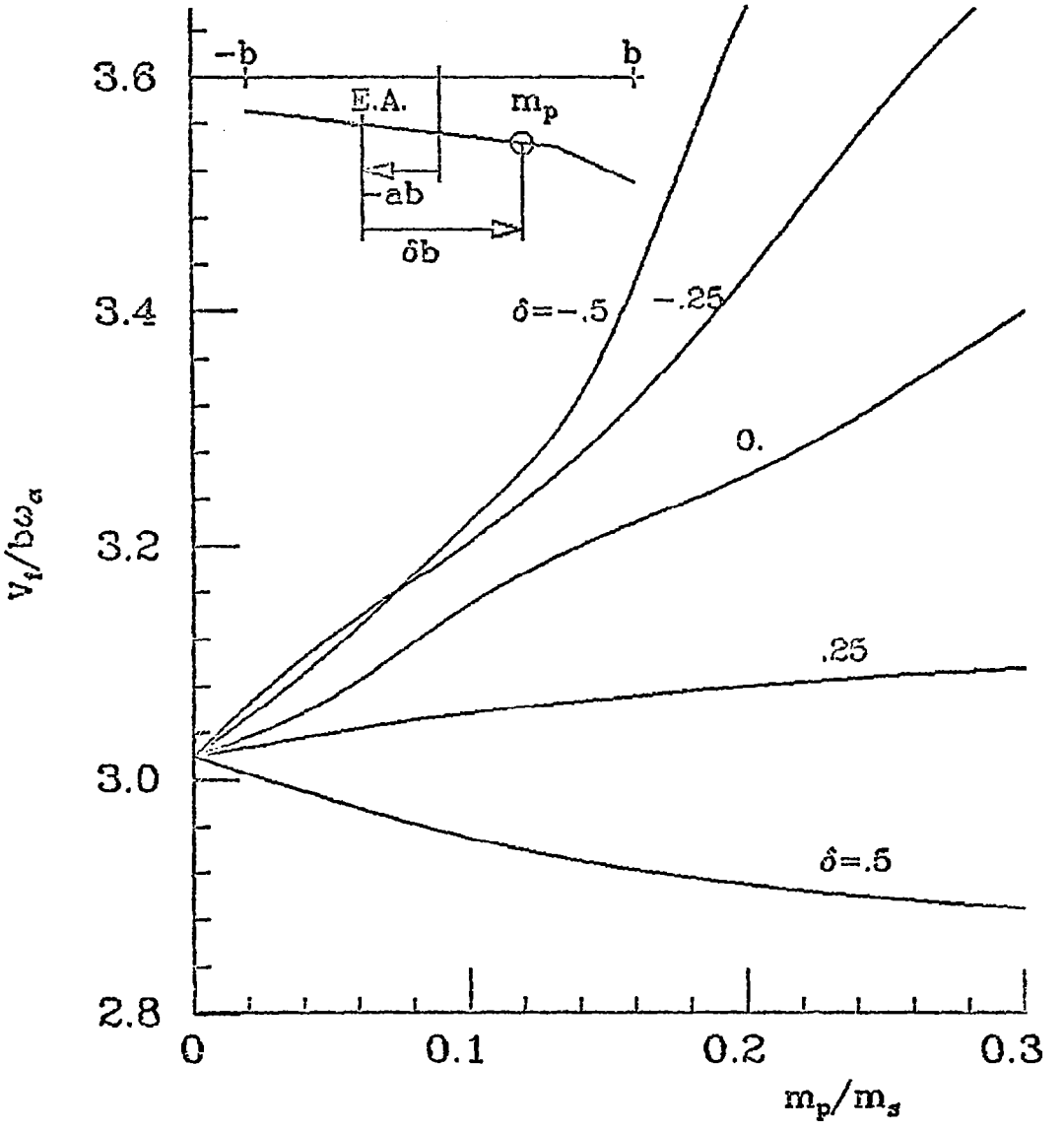

Figure 18: Variations of flutter speed with additional mass to the typical section at M = 0.

Other Passive Control Means

Other passive means that can be formulated as zero-order compensators are springs or dampers connecting two points with modal deflections $\{\Psi_{p1}\}$ and $\{\Psi_{p2}\}$.

For a linear spring with stiffness constant k_p, the coefficients of the control Eqs. (5.1),(5.2) and (5.7) are

$$\{G_2\} = \{\Psi_p\} \quad , \quad [H_d] = \{\Psi_p\}^t \quad , \quad [H_v] = 0 \quad ,$$
$$[H_a] = 0 \quad , \quad \{J\} = 0 \quad , \quad [C] = -k_p \quad \text{and} \quad [C_c] = 0 \tag{6.4}$$

where $\{\Psi_p\} = \{\Psi_{p1}\} - \{\Psi_{p2}\}$

A viscous damper with damping constant b_p is represented by

$$\{G_2\} = \{\Psi_p\} \quad , \quad [H_d] = 0 \quad , \quad [H_v] = \{\Psi_p\}^t \quad ,$$
$$[H_a] = 0 \quad , \quad \{J\} = 0 \quad , \quad [C] = -b_p \quad \text{and} \quad [C_c] = 0 \tag{6.5}$$

Unlike the concentrated mass, the spring and the damper have to connect points with significant relative motion in order to be effective. A useful application of pylon stiffness and damping tuning for wing-store flutter suppression is given in Ref. [42].

In some flutter cases, especially when the stability margin changes moderately with dynamic pressure, a reasonably-sized dynamic vibration absorber can be effective in suppressing flutter. A sketch of a dynamic vibration absorber, attached to the wing at a point with displacement $x_p = \{\Psi_p\}^t\{x\}$, is shown in Fig. 19. The equation of motion of m_p is

$$m_p\ddot{z}_p + b_p\dot{z}_p + k_p z_p = -m_p\ddot{x}_p \tag{6.6}$$

where $z_p = x_p' - x_p$

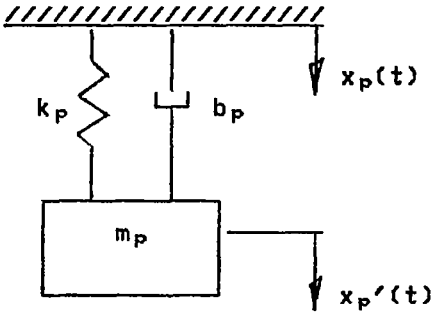

Figure 19: A sketch of a dynamic vibration absorber

In state-space form with $z_1 = z_p$ and $z_2 = \dot{z}_p$, Eq. (6.6) becomes

$$\begin{Bmatrix} \dot{z}_1 \\ \dot{z}_2 \end{Bmatrix} = \begin{bmatrix} 0 & 1 \\ -k_p/m_p & -b_p/m_p \end{bmatrix} \begin{Bmatrix} z_1 \\ z_2 \end{Bmatrix} + \begin{Bmatrix} 0 \\ -1 \end{Bmatrix} \ddot{x}_p \tag{6.7}$$

This is a second-order compensator as defined in Eq. (5.5). The dynamic vibration absorber can be thought of as a mechanical implementation of the control compensator and be treated as an active control system. As in the concentrated mass case, the open-loop state vector $\{z\}$ and

dynamic matrix $[F_1]$ remain untouched. The control variable is the force applied by the vibration absorber on the structure and the measurement is the acceleration at the mounting point. The coefficient matrices in Eqs. (5.1), (5.3), (5.5) and (5.7) are

$$\{G_2\} = \{\Psi_p\} \quad , \quad [H_0] = \{\Psi_p\}^t \quad ,$$

$$[A_c] = \begin{bmatrix} 0 & 1 \\ -k_p/m_p & -b_p/m_p \end{bmatrix} \quad , \quad [B_c] = \begin{Bmatrix} 0 \\ -1 \end{Bmatrix} \quad , \tag{6.8}$$

$$[C] = 0 \quad \text{and} \quad [C_c] = [k_p \; b_p]$$

The closed-loop equations (5.9) can now be constructed using the matrix relations of Eqs. (5.1), (5.4) and (5.8). The design parameters are the mounting location, which defines $\{\psi_p\}$, and the absorber parameters m_p, b_p and k_p. The cost-function definition and the optimization procedure can be carried out by the methods presented previously for active control, with a weighted mass-penalty term added to the cost function. To avoid excessive relative displacement z_p between the wing and m_p, the mean-square gust response of z_p can be included in the cost function by adding its weighted frequency response to $Z_d(i\omega)$ in Eq. (5.14). The frequency response of z_p is related to the model frequency response of Eq. (5.13) by

$$Z_p(i\omega) = \frac{\omega^2}{-\omega^2 + i2\zeta_p\omega_p\omega + \omega_p^2} \{\Psi_p\}^t \{X(i\omega)\} \tag{6.9}$$

where $\omega_p = \sqrt{k_p/m_p}$ and $\zeta_p = b_p/2m_p\omega_p$

The typical section in incompressible flow (see Fig. 1 and Table 2) was used to illustrate the effect of a dynamic vibration absorber. The changes in flutter velocity with the absorber uncoupled frequency ω_p, for various mounting locations δ (see Fig. 18), with $m_p/m_s = 0.2$ and $\zeta_p = 0.2$, are shown in Fig. 20.

When $\omega_p = 0$, m_p is not connected to the structure and the system is unaffected (Fig. 10). When $\omega_p \to \infty$, the flutter velocities approach those of the concentrated-mass case (Fig. 18). It is clear from Fig. 20 that a properly tuned vibration absorber is much more effective than a lumped mass. With $m_p/m_s = 0.2$, $\zeta_p = 0.2$ and $\delta = -0.5$, for example, the flutter velocity can be increased by 65%, compared with 20% in the concentrated-mass case. These results, however, are very sensitive to the absorber frequency tuning.

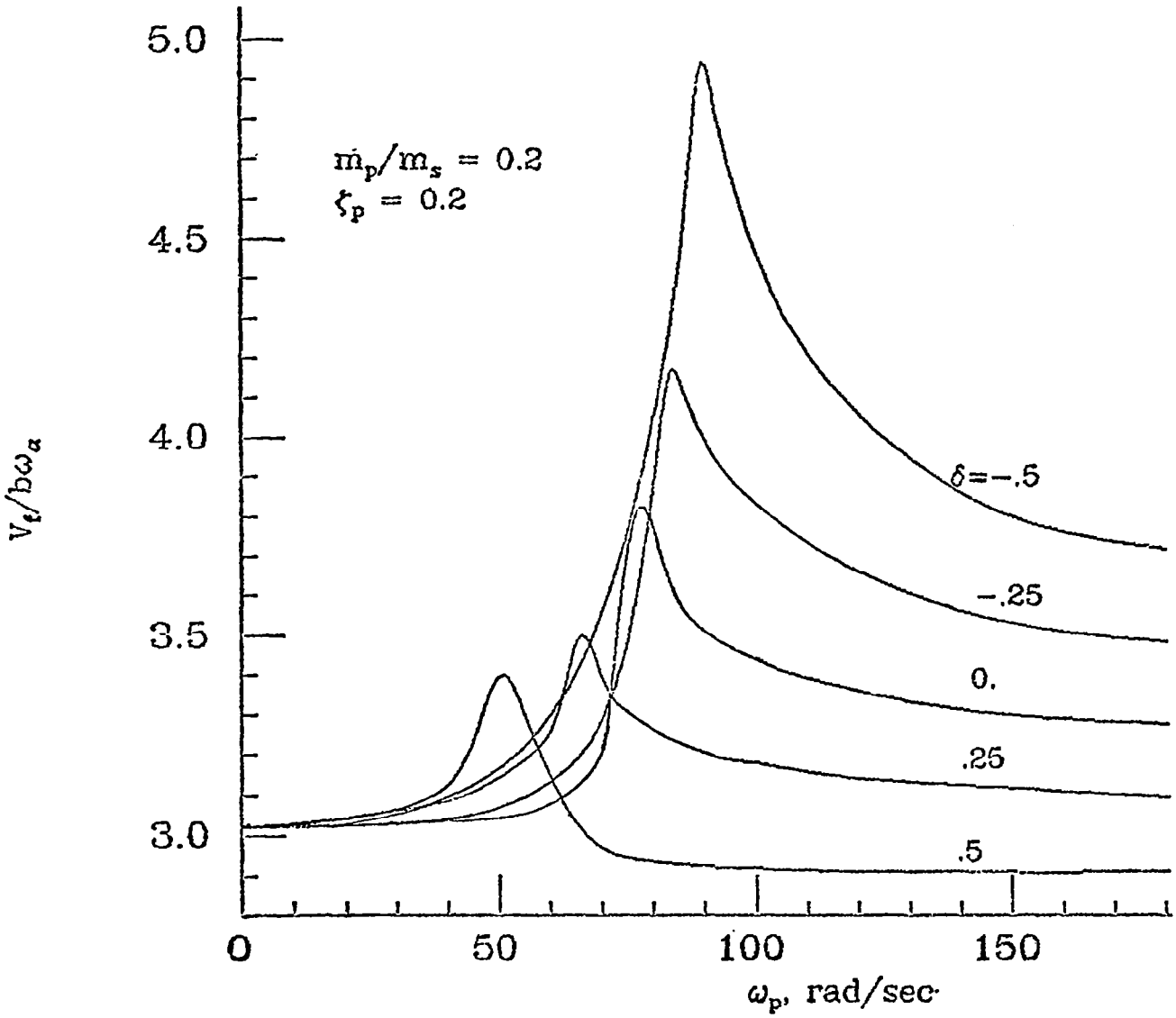

Figure 20: Variations of flutter speed with vibration-absorber frequency, typical section at M = 0.

CONCLUDING REMARKS

A review of the basic unsteady aerodynamic derivations and aeroelastic equations of motion which lead to the widely-used V-g method for flutter analysis has been presented. Based on the assumption that the wing undergoes simple harmonic motion, the V-g method gives correct results only for the flutter boundary flow conditions. Matched point solutions must be determined by iteration with density as a parameter.

Direct stability margin calculations at pre- and post-flutter conditions need aerodynamic influence coefficients for arbitrary motion. In order to solve the stability equations by the methods of linear algebra, the influence coefficients are approximated by rational functions of the nondimensionalized Laplace variable s'. Such approximations lead to constant coefficient, linear, finite state-space aeroelastic models.

Several rational approximation techniques are discussed, and a new "minimum-state" approximation method, which yields a minimal-order aeroelastic model for a given accuracy, is presented. All the methods consist of aerodynamic data calculated for oscillatory motion. The minimum-state method is first applied to a three-DOF typical section in incompressible flow. With two aerodynamic augmented states, the

approximated influence coefficients are within 5% of the "exact" Theodorsen coefficients in a range of $\pm 30°$ of the imaginary axis of the s' plane. Root loci of important structural modes usually fall within this range.

Application of the minimum-state method to the typical section at M = 0.7 and to the four-mode research wing model shows that, when the number of aerodynamic augmented states is similar to the number of degrees of freedom, all the approximated coefficients are within 5% of the exact ones along the imaginary axis. Off the imaginary axis there were no available data with which to compare the results. The minimum-state approximation is demonstrated to be significantly superior to Roger's and the matrix Padé approximants in terms of accuracy per model order. One disadvantage of the minimum-state method is that it is more complicated and computer time-consuming, because it involves solving nonlinear least-squares problems. This investment, however, pays off in repetitive flutter and control calculations.

It is shown that the minimum-state aeroelastic model can be used to design constant-parameter active control systems which by minimizing a cost function, defined as mean-square gust response over several flight conditions, assure stability over the entire flight envelope. Numerical examples for a typical section with a zero-order compensator and a research wing with a second-order compensator demonstrated the design procedure and showed a significant favorable change in the aeroelastic behavior with a single trailing edge control surface.

Finally, more traditional passive control means--such as concentrated masses, springs, dampers and dynamic vibration absorbers--are formulated as control input and output terms. They are shown to be analogous to active control means, making it possible to carry out simultaneously active and passive control analyses.

RECOMMENDATIONS

1. The minimum-state approximation should be applied to more aeroelastic systems in order to explore further its merits as compared with other rational approximation methods. The computation time might be reduced by finding more efficient solutions to the nonlinear least-squares problem stated in Eq. (4.27). Other improvements may be obtained by allowing the aerodynamic "open-loop" roots (the eigenvalues of $[R']$) to be complex.

2. Unsteady aerodynamic theory and computational algorithms should be further developed to provide aerodynamic influence coefficients in the entire s' plane for three-dimensional wings in compressible flow. This will enable checking the accuracy of the rational approximations off the imaginary axis of the Laplace domain. The minimum-state procedure should be modified to accommodate data for arbitrary s' values.

3. Rational approximations of the frequency-dependent gust loads and "coloring" of the gust velocity power spectral density should be attempted. This will add augmented states to the

aeroelastic model but will also enable replacement of the heavily time-consuming numerical integrations for the mean-square gust response by algebraic solution of Lyapunov equations [49].

4. The suggested active control design procedure should be compared with other flutter-suppression control techniques by applying them to the same mathematical models, wind-tunnel tests and flight test demonstrations.

5. The applicability of the control models developed in this study are not limited to the design of constant parameter, low-order continuous control systems. These models can be used in the design of other control systems, such as scheduled parameter systems, and in controllability, observability and sensitivity studies for choosing the control devices. The relatively low-order model has special potential for developing real-time, adaptive, digital control systems in which computation time is a critical parameter.

6. The merits of formulating passive flutter-suppression means as input and output control terms should be further explored by combining them with active control design and by applying them to the design of special flutter-related devices, such as decoupler pylons, control-surface mass balance and control-system actuators.

APPENDIX A

UNSTEADY AERODYNAMICS OF A TYPICAL SECTION IN INCOMPRESSIBLE FLOW

This appendix summarizes the unsteady aerodynamic loads on a typical section in incompressible flow due to arbitrary section motion and due to a disturbing gust with sinusoidal vertical velocity.

The unsteady aerodynamic loads on the typical section of Fig. 1 in two-dimensional incompressible flow due to oscillatory section motion were derived by Theodorsen [12] and generalized to arbitrary motion by Edwards [19], following Sears [18]. The Laplace transform of the loads reads

$$\{L_a(s)\} = q[A(s')]\{X(s)\} \tag{A.1}$$

where $\{x(t)\}^t = [h/b, \alpha, \beta]$, $\{L_a(t)\}^t = [-Lb, M_\alpha, M_\beta]$,

q is the dynamic pressure, s′ is the nondimensional Laplace variable sb/V, and [A(s′)] is the generalized aerodynamic influence coefficient matrix

$$[A(s')] = 2b^2\left([M_{nc}]s'^2 + \left[[B_{nc}]+C(s')\{R_1\}[S_2]\right]s' + [K_{nc}]+C(s')\{R_1\}[S_1]\right) \tag{A.2}$$

where the coefficient matrices are

$$[M_{nc}] = \begin{bmatrix} -\pi & \pi a & T_1 \\ \pi a & -\pi(a^2+1/8) & -T_{13} \\ T_1 & -T_{13} & T_3/\pi \end{bmatrix}$$

$$[B_{nc}] = \begin{bmatrix} 0 & -\pi & T_4 \\ 0 & \pi(a-\frac{1}{2}) & -T_{16} \\ 0 & -T_{17} & -T_{19}/\pi \end{bmatrix}$$

$$[K_{nc}] = \begin{bmatrix} 0 & 0 & 0 \\ 0 & 0 & -T_{15} \\ 0 & 0 & -T_{18}/\pi \end{bmatrix}$$

$$\{R_1\}^t = [-2\pi \quad 2\pi(a+\tfrac{1}{2}) \quad -T_{12}]$$

$$[S_1] = [\ 0 \quad 1 \quad T_{10}/\pi\ ]$$

$$[S_2] = [\ 1 \quad \tfrac{1}{2}-a \quad T_{11}/2\pi\ ]$$

and the constants are

$$T_1 = -(1/3)(2+c^2)\sqrt{1-c^2} + c\cos^{-1}c$$

$$T_3 = -(1/8)(1-c^2)(5c^2+4) + (1/4)c(7+2c^2)\sqrt{1-c^2}\cos^{-1}c - (c^2+1/8)(\cos^{-1}c)^2$$

$$T_4 = c\sqrt{1-c^2} = \cos^{-1}c$$

$$T_5 = -(1-c^2) - (\cos^{-1}c)^2 + 2c\sqrt{1-c^2}\cos^{-1}c$$

$$T_7 = (1/8)c(7+2c^2)\sqrt{1-c^2} - (c^2+1/8)\cos^{-1}c$$

$$T_8 = -(1/3)(1+2c^2)\sqrt{1-c^2} + c\cos^{-1}c$$

$$T_9 = \tfrac{1}{2}[(1/3)(1-c^2)^{3/2} + aT_4]$$

$$T_{10} = \sqrt{1-c^2} + \cos^{-1}c$$

$$T_{11} = (2-c)\sqrt{1-c^2} + (1-2c)\cos^{-1}c$$

$$T_{12} = \sqrt{1-c^2}(2+c) - (2c+1)\cos^{-1}c$$

$$T_{13} = -\tfrac{1}{2}[T_7 + (c-a)T_1]$$

$$T_{15} = T_4 + T_{10}$$

$$T_{16} = T_1 - T_8 - (c-a)T_4 + \tfrac{1}{2}T_{11}$$

$$T_{17} = -2T_9 - T_1 + (a-\tfrac{1}{2})T_4$$

$$T_{18} = T_5 - T_4T_{10}$$

$$T_{19} = -\tfrac{1}{2}T_4T_{11}$$

The generalized Theodorsen function is

$$C(s') = \frac{K_1(s')}{K_0(s')+K_1(s')} \qquad (A.3)$$

where K_n is a modified Bessel function of order n. Using Eq. (9.6.4) of Ref. [50] for $0 \leq \arg(s') \leq \pi$, Eq. (A.3) becomes

$$C(s') = \frac{H_1^{(2)}(z)}{H_1^{(2)}(z)+iH_0^{(2)}(z)} \qquad \text{where} \qquad z = -is' \qquad (A.4)$$

where $H_n^{(2)}$ is the Hankel function which is related to Bessel functions by

$$H_n^{(2)}(z) = J_n(z) - iY_n(z) \tag{A.5}$$

As indicated by Edwards [19], as $|s'| \to 0$, $C(s') \to 1$ independent of approach direction. To calculate $C(s')$, ascending power series of Bessel functions are derived from Eqs. (9.1.10) to (9.1.13) of Ref. [50].

$$J_0(z) = 1 + \sum_{j=1}^{\infty} \frac{(-z^2/4)^j}{(j!)^2} \tag{A.6}$$

$$Y_0(z) = \frac{2}{\pi}\left[\ln(z/2)+\gamma\right]J_0(z) - \frac{2}{\pi}\left[\sum_{j=1}^{\infty}\left[\frac{(-z^2/4)^j}{(j!)^2}\left(\sum_{m=1}^{j} 1/m\right)\right]\right] \tag{A.7}$$

where $\gamma = 0.577215665....$

$$J_1(z) = \frac{z}{2}\left[1 + \sum_{j=1}^{\infty} \frac{(-z^2/4)^j}{j!(j+1)!}\right] \tag{A.8}$$

$$Y_1(z) = \frac{2}{\pi}\left[-\frac{1}{z} + [\ln(z/2)+\gamma]J_1(z)\right] - \frac{z}{2\pi}\left[1 + \sum_{j=1}^{\infty}\left[2\left(\sum_{m=1}^{j} 1/m\right) + \frac{1}{j+1}\right]\frac{(-z^2/4)^j}{j!(j+1)!}\right] \tag{A.9}$$

The ascending series are converging very fast for the study range of interest $0 < |s'| \leq 2$.

The unsteady aerodynamic loads due to a disturbing gust with sinusoidal vertical velocity of amplitude w_g'' and frequency ω read

$$\{L_g(ik,t)\} = (q/V)\{A_g(ik)\}w_g''\exp(i\omega t) \tag{A.10}$$

where $k = \omega b/V$. The hinge and pitch components of the gust loads are given by Eq. (5-375) of Ref. [10]. In our notations, the related components of $\{A_g\}$ read

$$\begin{aligned} A_{g,1} &= -4\pi b^2\{C(ik)[J_0(k)-iJ_1(k)] + iJ_1(k)\} \\ A_{g,2} &= -(\tfrac{1}{2}+a)A_{g,1} \end{aligned} \tag{A.11}$$

For a relatively stiff actuator, and when the open-loop gust-induced hinge moments are not of particular interest, their effect is negligible and it is assumed that $A_{g,3} = 0$.

REFERENCES

1. Burris, P.M. and M.A. Bender, "Aircraft Load Alleviation and Mode Stabilization (LAMS)," AFFDL-TR-68-161, November 1969.

2. Murrow, H.N. and C.V. Eckstrom, "Drones for Aerodynamic and Structural Testing (DAST)--A Status Report," J. Aircraft, Vol. 16, No. 8, pp. 521-526, August 1979.

3. Roger, K.L., G.E. Hodges and L. Felt, "Active Flutter Suppression-- A Flight Test Demonstration," J. Aircraft, Vol. 12, No. 6, pp. 551-556, June 1975.

4. Nissim, E. and I. Abel, "Development and Application of an Optimization Procedure for Flutter Suppression Using the Energy Concept," NASA TP 1137, February 1978.

5. Hwang, C., B.A. Winther, G.R. Mills, T.E. Noll and M.G. Farmer, "Demonstration of Aircraft Wing/Store Flutter Suppression Systems," J. Aircraft, Vol. 16, No. 8, pp. 557-563, August 1979.

6. Abel, Irving, "An Analytical Technique for Predicting the Characteristics of a Flexible Wing Equipped with an Active Flutter-Suppression System and Comparison with Wind-Tunnel Data," NASA TP 1367, 1979.

7. Peloubet, R.P., Jr. and R.L. Haller, "Feasibility Study for F-16 Flutter Suppression System," AFFDL-TR-78-113, September 1978.

8. Triplett, W.E., "Active Flutter Suppression Systems for Military Aircraft, A Feasibility Study," AFFDL-TR-72-116, February 1973.

9. O'Connell, R.F. and A.F. Messina, "Design, Development and Testing of an Active Flutter Margin Augmentation System for a Commercial Transport Airplane," AIAA Paper No. 79-0790, April 1979.

10. Bisplinghoff, R.L., H. Ashley and R.L. Halfman, Aeroelasticity, Addison-Wesley, MA, 1955.

11. Przemieniecki, J.S., Theory of Matrix Structural Analysis, McGraw-Hill, NY, 1968.

12. Theodorsen, Theodore, "General Theory of Aerodynamic Instability and the Mechanism of Flutter," NACA Report No. 496, 1935.

13. Timman, T. and A.I. Van der Vooren, "Theory of the Oscillating Wing with Aerodynamically Balanced Control Surface in Two-Dimensional, Subsonic, Compressible Flow," National Luchtvaart-laboratorium, Amsterdam, Report No. F.54, 1949.

14. Garrick, I.E. and S.I. Rubinow, "Flutter and Oscillating Air-force Calculations for an Airfoil in Two-Dimensional Supersonic Flow," NACA Report No. 846, 1946. (Supersedes NACA TN 1158.)

15. Albano, E. and W.P. Rodden, "A Doublet-Lattice Method for Calculating Lift Distributions of Oscillating Surfaces in Subsonic Flow," AIAA J., Vol. 7, No. 2, pp. 279-285, February 1969.

16. Bisplinghoff, R.L. and H. Ashley, Principles of Aeroelasticity, Wiley and Sons, NY, 1962.

17. Smilg, Benjamin and Lee S. Wasserman, "Application of Three-Dimensional Flutter Theory to Aircraft Structures," ACTR No. 4798, Material Div., Army Air Corps, Jul. 9, 1942.

18. Sears, W.R., "Operational Methods in the Theory of Airfoils in Non-Uniform Motion," J. Franklin Inst., Vol. 230, No. 1, pp. 95-111, July 1940.

19. Edwards, John William, "Unsteady Aerodynamic Modeling and Active Aeroelastic Control," SUDAAR 504 (NASA Grant NGL-05-020-007), Stanford University, February 1977. (Available as NASA CR-148019.)

20. Edwards, J. W., "Applications of Laplace Transform Methods to Airfoil Motion and Stability Calculations," AIAA Paper No. 79-0772, April 1979.

21. Jones, Robert T., "The Unsteady Lift of a Wing of Finite Aspect Ratio," NACA Report No. 681, 1940.

22. Baker, G.A.,Jr., Essentials of Padé Approximants, Academic Press, NY, 1974.

23. Roger, K.L., "Airplane Math Modeling Methods for Active Control Design," AGARD-CP-228, August 1977.

24. Vepa, Ranjan, "Finite State Modeling of Aeroelastic Systems," NASA CR-2779, 1977.

25. Pratt, K.G., "Response of Flexible Airplanes to Atmospheric Turbulence," Performance and Dynamics of Aerospace Vehicles, NASA SP-258, pp. 439-503, 1971.

26. Hinze, J.O., Turbulence, McGraw-Hill, NY, 1959.

27. Dryden, H.L., "A Review of the Statistical Theory of Turbulence," Quart. Appl. Math., No. 1, 1943.

28. von Karman, Th., "Progress in the Statistical Theory of Turbulence," J. Marine Research, No. 7, 1948.

29. Federal Aviation Regulations, Part 25, Airworthiness Standards, Transport Category Airplanes.

30. Nissim, E., "Recent Advances in Aerodynamic Energy Concept for Flutter Suppression and Gust Alleviation Using Active Controls," NASA TN D-8519, September 1977.

31. Abel, I., B. Percy III and H.N. Murrow, "Two Synthesis Techniques Applied to Flutter Suppression on a Flight Research Wing," J. Guidance and Control, Vol. 1, No. 5, pp. 340-346, September 1978.

32. Wykes, J.H., "Active Flutter Suppression on an Aeroelastically Tailored HiMAT Vehicle," AFFDL-TR-79-3012, February 1979.

33. Newsom, Jerry R., "A Method for Obtaining Practical Flutter Suppression Control Laws Using Results of Optimal Control Theory," NASA TP-1471, August 1979.

34. Bryson, A.E., Jr. and Yu-Chi Ho, Applied Optimal Control, Halsted Press, NY, 1975,

35. Ashkenazi, A., "Parameter Insensitive Controllers," SUDAAR 520, Stanford University, May 1980.

36. Fletcher, R. and C.M. Reeves, "Function Minimization by Conjugate Gradients," Computer J., Vol. 6, pp. 149-154, July 1963.

37. Davidon, William C., "Variable Metric Method for Minimization," AEC Research and Development Report, ANL-5990 Rev. (Contract W-31-109-eng-38), U.S. At. Energy Comm., Nov. 1959.

38. Fletcher, R. and M.J.D. Powell, "A Rapidly Convergent Descent Method for Minimization," Computer J., Vol. 6, pp. 163-168, 1963.

39. Stewart, G.W., "A Modification of Davidon's Minimization Method to Accept Difference Approximations of Derivatives," J. Assoc. Comp. Mach., Vol. 14, pp. 72-83, January 1967.

40. Markowitz, J. and G. Isakson, "FASTOP-3: A Strength, Deflection and Flutter Optimization Program for Metallic and Composite Structures," AFFDL-TR-78-50, Vols. I and II, May 1978.

41. Haftka, R.T. and J.H. Starnes, Jr., "A Comparison of Two Types of Structural Optimization Procedures for Satisfying Flutter Requirements," AIAA Paper No. 74-405, April 1974.

42. Reed, W.H., III, J.T. Foughner and H.L. Runyan, "Wing/Store Decoupler Pylon: A Passive Flutter Suppression Concept," AIAA Paper No. 79-0791, April 1979.

43. Landahl, M.T., "Kernel Function for Nonplanar Oscillating Surfaces in a Subsonic Flow," AIAA J., Vol. 5, No. 5, pp. 1045-1046, May 1967.

44. Van der Vooren, A.I., "Collected Tables and Graphs," Manual of Aeroelasticity, Vol. IV, AGARD, January 1964.

45. Franklin, G.F. and J.D. Powell, Digital Control of Dynamic Systems, Addison-Wesley, 1980.

46. Nissim, E. and I. Lottati, "Active Control Systems for Flutter Suppression and Gust Alleviation in Supersonic Cruise Aircraft," AIAA Paper No. 79-0792, April 1979.

47. Gantmakher, F.R., Theory of Matrices, Chelsea Publications, NY, 1959.

48. Ferziger, J.H., Numerical Methods for Engineering Applications, ME200C Class Notes, Stanford University, March 1978.

49. Kailath, T., Linear Systems, Prentice-Hall, 1980.

50. Abramowitz, M. and I.A. Stegun, Handbook of Mathematical Functions, National Bureau of Standards, AMS 55, issued June 1965, Tenth Printing December 1972.

1. Report No.	2. Government Accession No.	3. Recipient's Catalog No.
NASA CR-3482		

4. Title and Subtitle	5. Report Date
DESIGN FOR ACTIVE AND PASSIVE FLUTTER SUPPRESSION AND GUST ALLEVIATION	November 1981
	6. Performing Organization Code
7. Author(s)	8. Performing Organization Report No.
Mordechay Karpel	
	10. Work Unit No.
9. Performing Organization Name and Address	11. Contract or Grant No.
Stanford University Department of Aeronautics and Astronautics Stanford, CA 94305	NGL-05-020-243
	13. Type of Report and Period Covered
12. Sponsoring Agency Name and Address	Contractor Report
National Aeronautics and Space Administration Washington, DC 20546	14. Sponsoring Agency Code

15. Supplementary Notes

Adapted from Ph. D. Dissertation, August 1980
Langley Technical Monitor: Robert V. Doggett, Jr.
Topical Report

16. Abstract

Analytical design techniques for active and passive control of aeroelastic systems are presented. These techniques are based on a rational approximation of the unsteady aerodynamic loads in the entire Laplace domain, which yields matrix equations of motion with constant coefficients. Some existing rational approximation schemes are reviewed, the matrix Pade approximant is modified, and a new technique which yields a minimal number of augmented states for a desired accuracy is presented. The state-space aeroelastic model is used to design an active control system for simultaneous flutter suppression and gust alleviation. The design target is for a continuous controller which transfers some measurements taken on the vehicle to a control command applied to a control surface. The control parameters are constant and they are optimized to minimize any desired combination of gust response parameters in a way that assures stability over the range of varying aerodynamic parameters in the entire flight envelope. Structural modifications are formulated in a way which enables the treatment of passive flutter suppression system with the same procedures by which active control systems are designed.

17. Key Words (Suggested by Author(s))	18. Distribution Statement
Active Controls Flutter Suppression Gust Alleviation Aeroelasticity	Unclassified - Unlimited Subject Category 08

19. Security Classif. (of this report)	20. Security Classif. (of this page)	21. No. of Pages	22. Price
Unclassified	Unclassified	115	A06

For sale by the National Technical Information Service, Springfield, Virginia 22161

NASA-Langley, 1981